

1-1-1991

## An analytical approach to quantum mechanical tunneling time in electronic devices

Prabhakaran Thanikasalam  
*University of Nevada, Las Vegas*

Follow this and additional works at: <https://digitalscholarship.unlv.edu/rtds>

---

### Repository Citation

Thanikasalam, Prabhakaran, "An analytical approach to quantum mechanical tunneling time in electronic devices" (1991). *UNLV Retrospective Theses & Dissertations*. 222.

<http://dx.doi.org/10.25669/0zir-r6uz>

This Thesis is protected by copyright and/or related rights. It has been brought to you by Digital Scholarship@UNLV with permission from the rights-holder(s). You are free to use this Thesis in any way that is permitted by the copyright and related rights legislation that applies to your use. For other uses you need to obtain permission from the rights-holder(s) directly, unless additional rights are indicated by a Creative Commons license in the record and/or on the work itself.

This Thesis has been accepted for inclusion in UNLV Retrospective Theses & Dissertations by an authorized administrator of Digital Scholarship@UNLV. For more information, please contact [digitalscholarship@unlv.edu](mailto:digitalscholarship@unlv.edu).

## INFORMATION TO USERS

This manuscript has been reproduced from the microfilm master. UMI films the text directly from the original or copy submitted. Thus, some thesis and dissertation copies are in typewriter face, while others may be from any type of computer printer.

**The quality of this reproduction is dependent upon the quality of the copy submitted.** Broken or indistinct print, colored or poor quality illustrations and photographs, print bleedthrough, substandard margins, and improper alignment can adversely affect reproduction.

In the unlikely event that the author did not send UMI a complete manuscript and there are missing pages, these will be noted. Also, if unauthorized copyright material had to be removed, a note will indicate the deletion.

Oversize materials (e.g., maps, drawings, charts) are reproduced by sectioning the original, beginning at the upper left-hand corner and continuing from left to right in equal sections with small overlaps. Each original is also photographed in one exposure and is included in reduced form at the back of the book.

Photographs included in the original manuscript have been reproduced xerographically in this copy. Higher quality 6" x 9" black and white photographic prints are available for any photographs or illustrations appearing in this copy for an additional charge. Contact UMI directly to order.

# U·M·I

University Microfilms International  
A Bell & Howell Information Company  
300 North Zeeb Road, Ann Arbor, MI 48106-1346 USA  
313/761-4700 800/521-0600



**Order Number 1350565**

**An analytical approach to quantum mechanical tunneling time  
in electronic devices**

**Thanikasalam, Prabhakaran, M.S.**

**University of Nevada, Las Vegas, 1992**

**U·M·I**  
300 N. Zeeb Rd.  
Ann Arbor, MI 48106



AN ANALYTICAL APPROACH TO QUANTUM  
MECHANICAL TUNNELING TIME IN ELECTRONIC  
DEVICES

by

Prabhakaran Thanikasalam

A thesis submitted in partial fulfillment  
of the requirements for the degree of

Master of Science  
in  
Electrical and Computer Engineering

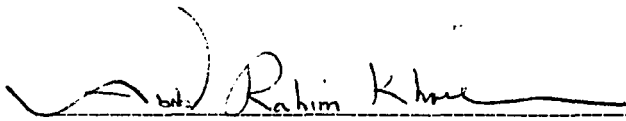
Department of Electrical and Computer Engineering  
University of Nevada, Las Vegas

August, 1992

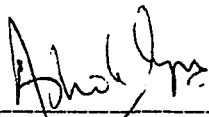
The thesis of Prabhakaran Thanikasalam for the degree of Master of Science  
in Electrical and Computer Engineering is approved.



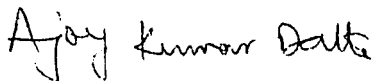
Chairperson. R. Venkatasubramanian, Ph.D



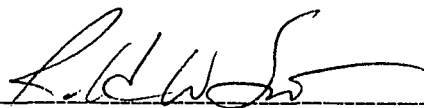
Examining Committee Member. Abdol Rahim Khoie, Ph.D



Examining Committee Member, Ashok Iyer, Ph.D



Graduate Faculty Representative. Ajoy Kumar Datta, Ph.D



Graduate Dean, Ronald W. Smith, Ph.D

University of Nevada, Las Vegas

August, 1992

## ABSTRACT

Starting from the analytical solution to the Time-Independent Schrödinger Equation, and exploiting the analogy between the transmission line equations and the time-independent Schrödinger wave equation, an analytical expression for the Average Particle Traversal (APT) time,  $\tau_{APT}$ , through a rectangular potential barrier region, under no bias, is derived, in terms of the barrier width, potential, and the incident energy of the electron. This approach is extended to derive an analytical expression for the APT time through a resonant tunneling structure, two symmetrical rectangular potential barriers sandwiching a potential well, under no bias. The results of the single potential barrier traversal time are compared with that of other approaches. The APT time is inversely proportional to the transmission coefficient, and satisfies physically intuitive energy limits. For the resonant tunneling structure, the APT time is minimum at resonant energies, and the  $\tau_{APT}$  is inversely proportional to the transmission coefficient. The maximum frequency of oscillation is estimated and compared for some of the experimentally studied resonant tunneling structures based on the APT time. The agreement is excellent.



## ACKNOWLEDGMENTS

I sincerely thank my major professor Dr. Venkatasubramanian for his direction, mystical talent of making the most difficult and subtle problems seem trivial, and for his incredible patience and endurance in clarifying most of my ideas. I also thank Dr. Abdol Rahim Khoie for several discussions, that I had with him, during the course of my study. I thank Dr. Marc Cahay of University of Cincinnati for a number of stimulating indirect discussions and advice.

I thank Dr. Ashok Iyer for financially supporting me through the Summer of 1991, during which I was able to complete most parts of my thesis. Sincere thanks are due to Dr. Ajoy Kumar Datta for serving on my thesis committee. I am grateful to Dr. Changfeng Chen and Dr. Stephen Lepp of the Physics Department for the discussions I had with them during the course of this research which gave us the confidence that we were proceeding in the right direction.

Finally, I wish to express my great appreciation for the gestures of my friends and confidants for their constructive and sometimes-tormenting criticisms which really kept me going, and above all, prevented me from feeling bored and lonely.

# Contents

Abstract . . . . .	iii
Acknowledgments . . . . .	iv
<b>1 INTRODUCTION</b>	<b>1</b>
1.1 Quantum Mechanics and Schrödinger's Wave Equation . . . . .	1
1.2 Tunneling Phenomena . . . . .	2
1.3 Resonant Tunneling Phenomena . . . . .	4
1.4 Overview of the Thesis . . . . .	6
<b>2 LITERATURE OVERVIEW</b>	<b>7</b>
2.1 Dwell Time . . . . .	7
2.2 Phase-delay Time . . . . .	8
2.3 Buttiker-Landauer Time . . . . .	9
2.4 Collins-Barker Monte-Carlo Simulation Time . . . . .	9
2.5 Average Particle Traversal (APT) Time . . . . .	10
<b>3 THEORETICAL FORMULATION</b>	<b>11</b>
3.1 Introduction . . . . .	11
3.2 Formalism . . . . .	11
3.3 Transmission Line Analogy . . . . .	13
3.3.1 The Quantum Mechanical Wave Impedance . . . . .	14
3.3.2 Steady State Probability Current Density . . . . .	15
3.3.3 Average Particle Traversal Time . . . . .	16

<b>4 SINGLE BARRIER</b>	<b>17</b>
4.1 Calculation of the Complex Coefficients of Wave Function Solutions . . . . .	17
4.2 APT Time Expression for the Single Barrier . . . . .	20
4.2.1 The APT Time for $E < V_o$ . . . . .	21
4.2.2 The APT Time for $E > V_o$ . . . . .	21
4.3 Various energy limits of $\tau_{APT}$ . . . . .	22
<b>5 DOUBLE BARRIER</b>	<b>24</b>
5.1 Calculation of the Complex Coefficients of Wave Function Solutions . . . . .	24
5.2 The $\tau_{APT}$ for a Resonant Tunneling Structure . . . . .	26
5.2.1 The $\tau_{APT}$ for the Left Barrier Region . . . . .	27
5.2.2 The $\tau_{APT}$ for the Potential Well Region . . . . .	28
5.2.3 The $\tau_{APT}$ for the Right Barrier Region . . . . .	29
<b>6 RESULTS, COMPARISONS and DISCUSSIONS</b>	<b>31</b>
6.1 Single Barrier . . . . .	31
6.1.1 Comparison of Dwell time, Phase-delay time, Buttiker-Landauer time, $\tau_{APT}$ , and the Classical time for, $E < V_o$ . . . . .	32
6.1.2 Comparison of Dwell time, Phase-delay time, Buttiker-Landauer time, $\tau_{APT}$ , and the Classical time for $E > V_o$ . . . . .	32
6.1.3 Effect of the barrier width on the $\tau_{APT}$ . . . . .	33
6.2 Double Barrier . . . . .	34
6.2.1 Comparison of $\tau_{APT}$ with Experimental Results . . . . .	34
6.2.2 Effect of barrier width on the APT time . . . . .	35
6.2.3 Effect of well width on the APT time . . . . .	36
<b>7 CONCLUSION</b>	<b>56</b>
<b>BIBLIOGRAPHY</b> . . . . .	<b>57</b>
<b>8 APPENDIX A</b>	<b>63</b>
8.1 Complex Coefficients of Wave Function Solutions . . . . .	63

# List of Figures

1.1	Quantum mechanical tunneling: (a) potential barrier of height $V_o$ and thickness $W$ ; (b) wave function $\Psi$ for an electron with energy $E < V_o$ , indicating a non zero value of the wave function beyond the barrier . . . . .	3
1.2	The I-V characteristics of a tunnel diode. <b>a-b</b> is the linear resistance region; <b>b-c</b> is the negative differential resistance, (NDR), region; and <b>c-d</b> is the exponential region. $I_p$ and $I_v$ are the peak and valley current. $V_p$ and $V_f$ are the peak and forward voltage, respectively. . . . .	3
1.3	Quantum mechanical tunneling in a resonant tunneling structure with a barrier width of $b$ and well width of $w$ . . . . .	4
3.1	Transmission line analogy: (a) transmission line circuit equivalent with a load impedance of $Z_L$ , (b) quantum mechanical system with a potential step barrier configuration. . . . .	12
4.1	Conduction band edge profile for a single rectangular potential barrier with the corresponding wave function solution for different regions. . . . .	18
5.1	Conduction band edge profile for a symmetrical double rectangular potential barrier with the wave function solutions for different regions. . . . .	25
6.1	The conduction band edge profile of a single rectangular potential barrier of width $200\text{\AA}$ and height $0.3eV$ . . . . .	37

6.2	Plot of the (a) Transmission Coefficient, and the (b) APT time, for a single rectangular potential barrier for $E < V_o$ , with barrier width $200\text{\AA}$ and barrier height $0.3eV$ . . . . .	38
6.3	Plot of the (a) Transmission Coefficient, and the (b) APT time, for a single rectangular potential barrier for $E > V_o$ , with barrier width $200\text{\AA}$ and barrier height $0.3eV$ . . . . .	39
6.4	Plot of the Traversal Times : (a) Dwell Time, (b) Phase-Delay Time, (c) Buttiker-Landauer Time, (d) APT time, and (e) Classical Time for $E < V_o$ , with barrier width $200\text{\AA}$ and barrier height $0.3eV$ . . . . .	40
6.5	Plot of the Traversal Times : (a) Dwell Time, (b) Phase-Delay Time, (c) Buttiker-Landauer Time, (d) APT time, and (e) Classical Time for $E > V_o$ , with barrier width $200\text{\AA}$ and barrier height $0.3eV$ . . . . .	41
6.6	Plot of the Traversal Times : (a) Dwell Time, (b) Phase-Delay Time, (c) Buttiker-Landauer Time, (d) APT time, (e) Classical Time, and the (f) Transmission Coefficient for $E > V_o$ , with barrier width $200\text{\AA}$ and barrier height $0.3eV$ . . . . .	42
6.7	3-Dimensional surface plot of the APT time, for the case of $E < V_o$ with the barrier height $1.0eV$ and barrier width in the range $25\text{\AA}$ to $250\text{\AA}$ . . . . .	43
6.8	3-Dimensional surface plot of the APT time, for the case of $E > V_o$ with the barrier height $1.0eV$ and barrier width in the range $25\text{\AA}$ to $250\text{\AA}$ . . . . .	44
6.9	The conduction band edge profile of a symmetrical double rectangular potential barrier structure with a barrier height of $0.956eV$ , barrier width of $30\text{\AA}$ and a well width of $100\text{\AA}$ . . . . .	45
6.10	Plot of the (a) Transmission Coefficient and the (b) APT time for a symmetrical double rectangular potential barrier structure with a barrier height $0.956eV$ , barrier width $30\text{\AA}$ and a well width $100\text{\AA}$ , for $E < V_o$ . . . . .	46
6.11	The conduction band edge profile of a symmetrical double rectangular potential barrier structure with a barrier height $0.23eV$ , barrier width $50\text{\AA}$ and a well width $50\text{\AA}$ . . . . .	47

6.12	Plot of the (a) Transmission Coefficient and the (b) APT time for a symmetrical double rectangular potential barrier structure with a barrier height $0.23eV$ , barrier width $50\text{\AA}$ and a well width $50\text{\AA}$ , for $E < V_o$ . . . . .	48
6.13	The conduction band edge profile of a symmetrical double rectangular potential barrier structure with a barrier height $1.0eV$ , barrier width $25\text{\AA}$ and a well width $45\text{\AA}$ . . . . .	49
6.14	Plot of the (a) Transmission Coefficient and the (b) APT time for $E < V_o$ for a symmetrical double rectangular potential barrier structure with a barrier height $1.0eV$ , barrier width $25\text{\AA}$ and a well width $45\text{\AA}$ . . . . .	50
6.15	The conduction band edge profile of a symmetrical rectangular double potential barrier structure of barrier height $0.3eV$ , barrier width in the range from $30\text{\AA}$ to $100\text{\AA}$ and well width $30\text{\AA}$ , for $E < V_o$ . . . . .	51
6.16	3-Dimensional surface plot of the APT time for $E < V_o$ . The barrier height is $0.3eV$ and the barrier width in the range from $30\text{\AA}$ to $100\text{\AA}$ and the well width is $30\text{\AA}$ . . . . .	52
6.17	The conduction band edge profile of a symmetrical rectangular double potential barrier structure of barrier height $1.0eV$ , barrier width $30\text{\AA}$ and the well width in the range from $30\text{\AA}$ to $110\text{\AA}$ . . . . .	53
6.18	3-Dimensional surface plot of the APT time for $E < V_o$ . The barrier height is $1.0eV$ and barrier width $30\text{\AA}$ and the well width in the range from $30\text{\AA}$ to $110\text{\AA}$ . . . . .	54
6.19	3-Dimensional surface plot of the (a) APT time and the (b) transmission coefficient for $E < V_o$ . The barrier height is $1.0eV$ and barrier width is $30\text{\AA}$ and well width in the range from $30\text{\AA}$ to $110\text{\AA}$ . . . . .	55

## Chapter 1

# INTRODUCTION

### 1.1 Quantum Mechanics and Schrödinger's Wave Equation

The **Schrödinger Equation** is analogous to a classical energy conservation equation, and describes the dynamics of a quantum particle. A quantum particle is one whose wavelength is very small compared to the dimensions of the system. When the dimensions of the dynamic system of the particle are extremely small, the classical mechanics does not explain many of the experimental observations, such as diffraction and tunneling. The Schrödinger equation was developed to explain these physical phenomena. The time-dependent Schrödinger equation in one-dimension for a quantum particle subjected to a potential,  $V(x)$ , is given by:

$$-\frac{\hbar^2}{2m^*} \frac{\partial^2 \Psi(x)}{\partial x^2} \Xi(t) + V(x) \Psi(x) \Xi(t) = -\frac{\hbar}{j} \Psi(x) \frac{\partial \Xi(t)}{\partial t}$$

where  $m^*$  is the effective mass of the particle,  $\hbar$  is the modified Planck's constant,  $\frac{\hbar}{2\pi}$ , and  $E$  is the energy of the particle. The time-independent Schrödinger equation which holds good when the total energy of the particle is independent of time, is given by:

$$\frac{d^2 \Psi(x)}{dx^2} + \frac{2m^*}{\hbar^2} [E - V(x)] \Psi(x) = 0$$

The boundary conditions are:  $\Psi_n(x \rightarrow \pm\infty) = 0$  and  $\Psi_n(x)$  and  $\Psi'_n(x)$  are continuous everywhere,  $-\infty < x < \infty$ . The number of solutions to this equation are infinite. The eigen values and functions are denoted with  $n$  as the index -  $E_n$  and  $\Psi_n(x)$ . The physical meaning of  $\Psi_n(x)$  is that  $|\Psi_n(x)|^2 dx$  provides the probability of finding the quantum particle between  $x$  and  $x + dx$  with unity probability of finding the particle in  $-\infty < x < \infty$ .

## 1.2 Tunneling Phenomena

In a single potential barrier comprising of *GaAs/AlAs/GaAs*, conduction band edge profile shown in Figure[1.1], as the height of the potential barrier is finite,  $\Psi_n$  is now zero at the *AlAs/GaAs* barrier interface.  $\Psi_n$  and  $\Psi'_n$  are continuous and non-zero at each boundary of the barrier, and  $\Psi_n$  and  $\Psi'_n$  are non-zero within and beyond the potential barrier. Since  $\Psi_n$  has a non-zero value to the right side of the barrier as shown in Figure[1.1],  $\Psi_n^* \Psi_n$  is non-zero, implying that the probability of finding the particle with  $E < V_o$  beyond the barrier region is finite. According to classical mechanics, the probability of finding the particle with  $E < V_o$  beyond the first *AlGaAs/GaAs* interface is zero, since such a real space transfer of the particle through a potential barrier region is prohibited classically. The physical mechanism by which the particle, with  $E < V_o$ , penetrating a finite potential barrier is called quantum mechanical tunneling through the barrier. The tunneling probability is directly related to the energy of the particle,  $E$ , relative to  $V_o$  and the barrier width,  $d$ .

The first device proposed, based on the tunneling phenomena, was the tunnel diode. The Tunnel diode is often called the Esaki diode after L. Esaki [20, 23], who in 1973 received the Nobel prize for his work on this effect. The basic structure is a  $p^+n^+$  diode with  $p$  and  $n$  regions are degenerately doped so that the depletion layer region is very thin. Due to thin depletion layer, electrons in the conduction band can tunnel through the thin depletion region to the valence band electrons. A tunnel diode exhibits the critical feature of negative differential resistance (NDR), over a portion of its  $I - V$  characteristics, as shown in Figure[1.2]. In NDR region, the  $I - V$  characteristics exhibits a negative slope. i.e., the quantity  $\frac{dI}{dV}$  is negative.



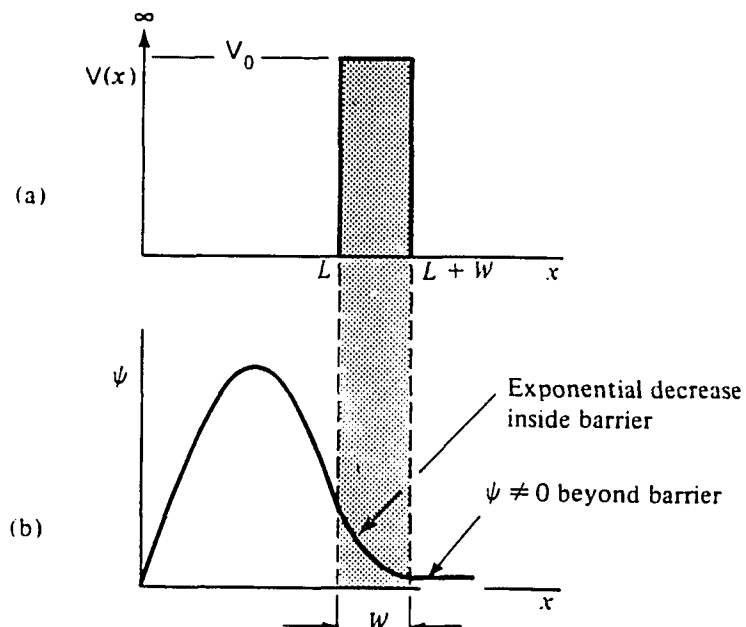


Figure 1.1: Quantum mechanical tunneling: (a) potential barrier of height  $V_0$  and thickness  $W$ ; (b) wave function  $\Psi$  for an electron with energy  $E < V_0$ , indicating a non zero value of the wave function beyond the barrier

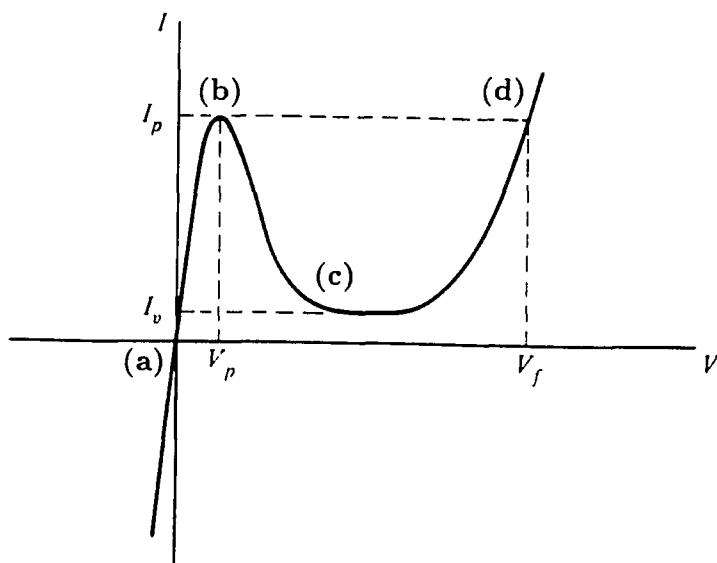


Figure 1.2: The I-V characteristics of a tunnel diode. a-b is the linear resistance region; b-c is the negative differential resistance, (NDR), region; and c-d is the exponential region.  $I_p$  and  $I_v$  are the peak and valley current.  $V_p$  and  $V_f$  are the peak and forward voltage, respectively.

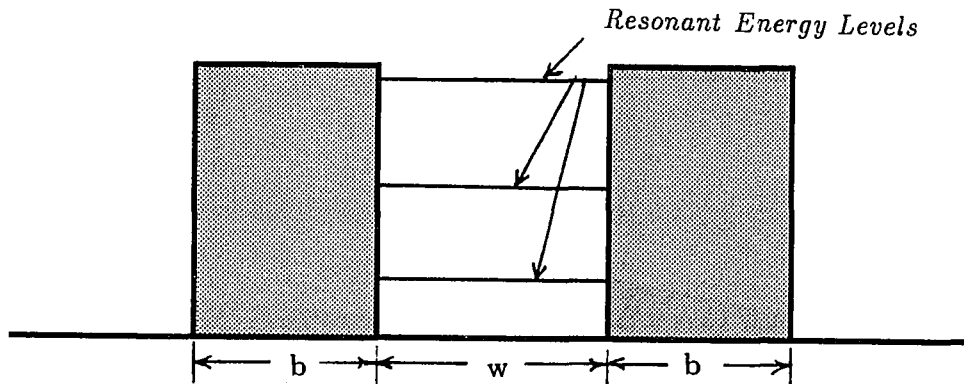


Figure 1.3: Quantum mechanical tunneling in a resonant tunneling structure with a barrier width of  $b$  and well width of  $w$ .

### 1.3 Resonant Tunneling Phenomena

With the advent of Molecular Beam Epitaxy (MBE), it is possible to grow thin layers of  $AlAs$  sandwiched between  $GaAs$ , thus creating a potential barrier in the conduction band edge profile, as shown in Figure[1.1]. The thickness of the  $AlAs$  layers can be as small as  $10\text{\AA}$ , which is 4 mono layers of  $AlAs$ . Double barrier structures as shown in Figure[1.3], successfully grown by MBE, in which a  $GaAs$  layer (well) is sandwiched between two  $AlAs$  barrier layers, quantized energy levels, dictated by quantum mechanics, exist within the well region. When the incident energy of the particle in the free propagating region outside the potential barrier equals one of the quantized energies, the transmission probability is unity, i.e., resonant tunneling results. For energy values other than the resonant ones, the transmission probability is less than unity. This is referred to as non-resonant tunneling phenomena.

R. Tsu and L. Esaki[20] proposed a superlattice structure in 1969 for application in negative differential resistance (NDR) devices. In 1972, L. Esaki *et. al.* reported for the first time, the observation of NDR in a  $GaAs/AlGaAs$  superlattice[22]. Two years later

L.L. Chang *et. al.*, observed NDR at temperature below  $77^\circ K$  in a double barrier resonant tunneling diode, i.e. two periods of a *GaAs/AlGaAs* superlattice.

In 1983, Sollner *et. al.*[48] reported a large NDR region in the  $I - V$  characteristics of *GaAs/AlGaAs* double barrier resonant tunneling device, with a peak-to-valley ratio of 6:1 at  $25^\circ K$ . Moreover, the current response measured at a driving frequency of 2.5 THz was remarkably similar to the response expected from DC measurements, indicating the potential for high frequency applications[25]. A year later, Sollner *et. al.* reported the first high frequency oscillations generated by a resonant tunneling device at frequencies up to 18 GHz[47]. In 1985, Shewchuk *et. al.* reported the first room temperature observation of the NDR in a *GaAs/AlGaAs* system[43, 44].

The demonstration of resonant tunneling phenomena has led to a number of proposals for devices with a third terminal to control the NDR characteristics. Capasso *et. al.* proposed a heterojunction bipolar transistor with a single quantum well in the base region [13, 14, 15]. There are other resonant tunneling devices proposed by Luryi *et. al.*[34], Ray *et. al.*[42] using MOCVD at  $300^0$  K. Tsuchiya *et. al.*[49] reported room-temperature observations of negative differential resistance in 1985.

Bonnefoi *et. al.*[5, 6], proposed a device; Negative Resistance Stark Effect Transistor (NERSET). This is a double barrier resonant tunneling device with an extra (base) contact. Since this base is shielded by a thick  $1000 - 1500\text{\AA}$  potential barrier, the base current is negligible. Nakata *et. al.* proposed a triode with a metal-insulator superlattice in the base, acting as an artificial semiconductor[35]. This device, called resonant electron transfer triode (RETT), is excted to perform well in high-speed applications because of low resistivity of metal contacts. Due to the periodicity of the metal-insulator superlattice, an artificial conduction band in the base region is formed. When the device is biased such that emitter Fermi level is aligned with the artificial conduction band in the base, electrons resonantly tunnel from emitter to collector.

Magnetic-field-induced resonant tunneling was discussed by Ramaglia *et. al.*[39]. Recent paper by Glazer *et. al.* discusses the case of tunneling through highly transparent double barriers[24]. Ranfagni *et. al.* reported delay-time measurements in narrow wave guides as a test of tunneling through single barrier[40, 41]. A thorough recount of the history of

resonant tunneling can be found in Reference[21].

In the context of tunneling devices, the two physical quantities of interest to device physicists and engineers are the tunneling current and the tunneling time. The subject of this thesis is the latter quantity, the tunneling time. Specifically, based on average particle velocity during tunneling, the tunneling time for a single and double barrier are studied. Henceforth, this tunneling time is called the Average Particle Traversal time or APT time.

## 1.4 Overview of the Thesis

A brief literature survey, discussing various theoretical approaches to tunneling times is presented in Chapter 2. The analogy between the solutions to the one-dimensional time-independent Schrödinger equation and transmission line equations is exploited and the derivation of APT time based on the analogy are discussed in Chapter 3. Analytical expressions for APT time for the case of a single potential barrier and a symmetrical double barrier under no bias are derived in Chapters 4 and 5, respectively. Results and discussion are presented in Chapter 6. Conclusions along with the proposal for future work are presented in Chapter 7.

## Chapter 2

# LITERATURE OVERVIEW

The prospect of high-speed devices based on resonant tunneling structures has brought new urgency to understand every aspect of tunneling phenomena for the formulation of the theory of dynamics of such systems. The question which is relevant to the dynamics of such a system and that has resulted in a wealth of literature is “**How long does it take for a particle to tunnel?**”.

The recent theoretical work on the tunneling times has centered around one-dimensional models. Within this limited area of research, there are at least six different approaches suggested in the literature. These approaches are : the dwell time[45], the phase-delay time[26, 50], the Buttiker-Landauer traversal time[7, 8, 9, 10], the complex traversal time[37, 38, 46], the Collins-Barker Monte-Carlo simulation time[16, 17, 18], and the Average Particle Traversal (APT) time. No two of these approaches agree[27, 28, 29, 32, 33]. . In this chapter, five approaches are reviewed and contrasted.

### 2.1 Dwell Time

The dwell time[45] is, in the context of the scattering of particles with fixed energy, the time spent in any finite region of space, averaged over all the incoming particles. Thus, the dwell

time can serve as a reference point in any discussion on tunneling times. This describes the average time a particle dwells within the barrier irrespective of it either reflects or transmits at the end of its stay. The dwell time,  $\tau_{dwell}$ , is defined as:

$$\tau_{dwell} = \frac{N}{J}$$

where  $N$  is the number of particles within the barrier region and  $J$  is the incident flux of the particles. The  $\tau_{dwell}$  for a single rectangular barrier can be shown to be equal to[7]:

$$\tau_{dwell} = \left( \frac{m^* k}{\hbar \alpha} \right) \frac{2\alpha d(\alpha^2 - k^2) + k_o^2 \sinh(2\alpha d)}{4k^2\alpha^2 + k_o^4 \sinh^2(\alpha d)}$$

where  $m^*$  is the effective mass,  $\hbar$  is the modified Planck's constant,  $\frac{\hbar}{2\pi}$ ,  $k = \sqrt{\frac{2m^*E}{\hbar^2}}$ ,  $\alpha = \sqrt{\frac{2m^*(V_o - E)}{\hbar^2}}$  and  $k_o = \sqrt{\frac{2m^*V_o}{\hbar^2}}$  with  $E$  being the energy of the incident electrons.  $V_o$  and  $d$  are the barrier height and width, respectively. The dwell time in a resonant tunneling structure is discussed by Pandey *et. al.* [36].

## 2.2 Phase-delay Time

The other well established tunneling time concept is the phase-delay time[26, 50]. A time delay for the scattering process can be calculated by following the peak of a wave packet via. the method of stationary phase[26]. Phase-delay time is the time interval between the time the peak of the incident wave enters the barrier and the time the peak of the transmitted wave appears beyond the barrier. The expression for the phase-delay time for single rectangular barrier is given by[7]:

$$\tau_{phase} = \left( \frac{m^*}{\hbar k \alpha} \right) \frac{2\alpha d k^2(\alpha^2 - k^2) + k_o^4 \sinh(2\alpha d)}{4k^2\alpha^2 + k_o^4 \sinh^2(\alpha d)}$$

A strong deformation of the wave packet will result when the wave packet interacts with a thick barrier. This deformation may shift the peak of the wave from  $k$  in the incident

wave to  $k'$  in the transmitted wave, with  $k \neq k'$ . Thus, the traversal time calculated by this method of following the peak of the wave packet becomes meaningless, as the same particle is not used for the time delay measurement.

### 2.3 Buttiker-Landauer Time

Buttiker and Landauer[7, 8, 9, 10] considered tunneling through time-dependent rectangular barrier with a small oscillating component added to the static barrier height. For a slowly varying potential, the additional time dependence of the transmitted wave is caused by the variation of the transmission probability with the height of the barrier. If the potential oscillates fast compared to the traversal time ( $\omega \gg 1/\tau$ ), then the particles see a time-independent barrier of average height  $V_0$ . For slowly varying potential ( $\omega \ll 1/\tau$ ), the tunneling particles see an effective time-dependent static barrier of height  $V(t)$ . Identifying the transition frequency at which the static barrier becomes an oscillating barrier for the particles, provides one with the inverse of a traversal time. The expression for Buttiker-Landauer traversal time for a single rectangular barrier is given as:

$$\tau_{B-L} = (\tau_{dwell}^2 + \tau_z^2)^{\frac{1}{2}}$$

where  $\tau_z$  is given by:

$$\tau_z = \left( \frac{m^* k_o^2}{\hbar \alpha^2} \right) \frac{(\alpha^2 - k^2) \sinh^2(\alpha d) + (k_o^2 d \alpha / 2) \sinh(2\alpha d)}{4k^2 \alpha^2 + k_o^4 \sinh^2(\alpha d)}$$

In this approach, the particles that are tunneling and those which are reflected are differentiated.

### 2.4 Collins-Barker Monte-Carlo Simulation Time

In this approach, a Gaussian wave packet with a particular standard deviation  $k$ , is made to impinge on a potential barrier and the time delay associated between the entrance of

the peak of the incident wave and the appearance of the peak of the transmitted wave beyond the potential barrier, is computed numerically [16, 17], using the conventional Monte-Carlo approach. Based on excellent agreement of Monte-Carlo time and phase-delay time, it was concluded that the phase-delay time result originally obtained by Wigner[50] and Hartman[26] is the best expression to use for a wide parameter range of barriers, energies and wave packets.

## 2.5 Average Particle Traversal (APT) Time

In this approach, an average tunneling velocity at steady state is defined as  $v_{av}(x) = \frac{J}{|\Psi(x)|^2}$ , with  $J$  being independent of  $x$ , and  $|\Psi(x)|^2$  is the probability density function at any point  $x$  along the barrier[31]. The analogy between the solution to the time-independent Schrödinger equation and the steady state transmission line equation for a loss-less homogeneous transmission line with a load, is exploited. A quantity analogous to the characteristic impedance of the transmission line called, Quantum Mechanical Wave Impedance (QMWI),  $Z(x)$ , is derived in terms of the complex coefficients of the solutions to the wave function as a function of  $x$ [3, 31]. The  $v_{av}(x)$  is then related to  $Z(x)$  and the APT time,  $\tau_{APT}$ , is obtained as:

$$\tau_{APT} = \int_0^d \frac{dx}{v_{av}(x)} \quad (2.1)$$

where  $d$  is the width of the barrier.

The integral expression given by Eq.[2.1] was used to obtain the tunneling time through a delta function by Anwar *et. al.*[4] numerically. The tunneling through an emitter-base junction of a Heterojunction Bipolar Transistor was investigated by Cahay *et. al.* using numerical integration of the Eq.[2.1][11, 12].



## Chapter 3

# THEORETICAL FORMULATION

### 3.1 Introduction

In this chapter, a discussion of the analogy between the the solution to the time-independent Schrödinger equation and transmission line equations in one-dimension are presented. Exploiting this analogy, a quantity called the Quantum Mechanical Wave Impedance (QMWI) is derived in terms of the wave function solutions. Using QMWI, the average tunneling velocity is derived and is used to derive the APT time,  $\tau_{APT}$ .

### 3.2 Formalism

Let a flux of electrons, with energy  $E$ , be incident on the potential barrier, as shown in Figure [3.1]. The dynamic equation governing the electron system is the time-dependent Schrödinger equation. The Schrödinger equation at steady state is given by:

$$\frac{d^2\Psi(x)}{dx^2} + \frac{2m^*}{\hbar^2}[E - V(x)]\Psi(x) = 0 \quad (3.1)$$

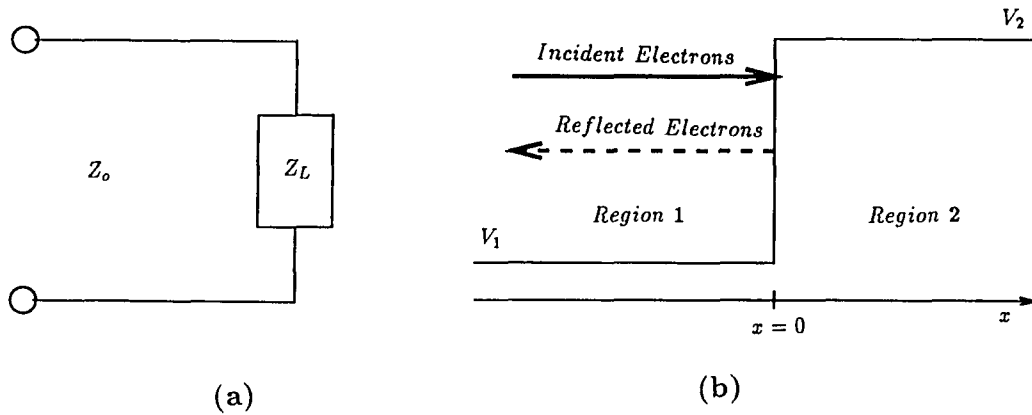


Figure 3.1: Transmission line analogy: (a) transmission line circuit equivalent with a load impedance of  $Z_L$ , (b) quantum mechanical system with a potential step barrier configuration.

The solution to this time-independent Schrödinger equation in region 1 with conduction band edge potential profile, as shown in Figure[3.1], can be written as:

$$\Psi(x) = A^+(e^{\alpha x} - \rho e^{-\alpha x}) \quad (3.2)$$

where  $\alpha = \gamma + j\beta = j\sqrt{\frac{2m^*(x)}{\hbar^2}(E - V_o)}$

$\rho$  is the wave amplitude reflection coefficient,  $\alpha$  is the propagation constant, and  $E$  is the energy of the incident electrons.  $\gamma$  and  $\beta$  are the real and imaginary parts of the propagation constant  $\alpha$ , respectively.

In particular, the wave equation for regions 1 and 2 can be written as:

$$\Psi_1(x) = A_1^+(e^{\alpha_1 x} - \rho e^{-\alpha_1 x}) \dots \dots x < 0 \quad (3.3)$$

$$\Psi_2(x) = A_2^+ e^{\alpha_2 x} \dots \dots x > 0 \quad (3.4)$$

respectively,

where  $\alpha_i = j\sqrt{\frac{2m_i^*}{\hbar^2}(E - V_i)} = \gamma_i + j\beta_i$

$m_i^*(x), V_i, (i = 1, 2)$  are the effective mass, and the potential, respectively, for the  $i^{th}$  region. Here,  $\gamma_i$  and  $\beta_i$  are the real and imaginary parts of the propagation constant  $\alpha_i$  for the  $i^{th}$  region.

There is no reflection of the wave in region  $x > 0$ , because the region is homogeneous and of infinite extent. Applying the boundary conditions at  $x = 0$ ,  $\Psi_1(x = 0) = \Psi_2(x = 0)$  and  $\Psi_1'(x = 0)/m_1^* = \Psi_2'(x = 0)/m_2^*$ , an expression for  $\rho$  is obtained as:

$$\rho = \frac{[\alpha_2/m_2^* - \alpha_1/m_1^*]}{[\alpha_2/m_2^* + \alpha_1/m_1^*]} \quad (3.5)$$

Differentiating Eq.[3.2] with respect to  $x$  and multiplying both sides of the equation by a factor  $\frac{\hbar}{jm^*}$ , an expression for  $\Phi(x)$  is obtained as:

$$\Phi(x) = \frac{\hbar}{jm^*} \frac{d\Psi(x)}{dx} = A^+ Z_0 (e^{\alpha x} + \rho e^{-\alpha x}) \quad (3.6)$$

where  $Z_0 = \frac{\alpha \hbar}{jm^*}$

### 3.3 Transmission Line Analogy

The expressions for voltage,  $V(x)$ , and current,  $I(x)$ , along the homogeneous lossless transmission line with generalized distributed impedance, are given by:

$$I(x) = I^+ (e^{\alpha x} - \Gamma_t e^{-\alpha x}) \quad (3.7)$$

$$V(x) = I^+ Z_0 (e^{\alpha x} + \Gamma_t e^{-\alpha x}) \quad (3.8)$$

where

$$\Gamma_t = \left[ \frac{Z_L - Z_0}{Z_L + Z_0} \right]$$

where  $\Gamma_t$  is the wave amplitude reflection coefficient.

$Z_L$  and  $Z_O$  are the load and characteristic impedance of the transmission line, respectively. Comparing the expressions for  $\Psi(x)$  and  $\Phi(x)$  given by Eqs.[3.2] and [3.6] respectively, with the expressions for  $I(x)$  and  $V(x)$  for transmission line given by Eqs.[3.7] and [3.8], respectively, it is observed that they are analogous.  $Z_O$  in Eq.[3.2] and [3.6] is the quantum mechanical analog of the characteristic impedance of the transmission line,  $Z_O$  given by,  $-\sqrt{Z/Y}$  where  $Z$  and  $Y$  are the series impedance and the shunt admittance, per unit length of the transmission line, respectively.

### 3.3.1 The Quantum Mechanical Wave Impedance

At any plane  $x$ , the Quantum Mechanical Wave Impedance (QMWI) [31] can be obtained from Eq.[3.2] and [3.6] as:

$$Z(x) = \frac{\Phi(x)}{\Psi(x)} \quad (3.9)$$

$Z(x)$  can be re-written as:

$$\frac{2\hbar}{jm^*(x)} \frac{\Psi'(x)}{\Psi(x)} = Z(x) = R(x) + jX(x) \quad (3.10)$$

where  $R(x)$  and  $X(x)$  are the real and imaginary parts of  $Z(x)$  at any point  $x$ , looking in the positive  $x$  direction.

Multiplying both sides of Eq.[3.10] by  $\frac{jm^*(x)}{2\hbar}$ , Eq.[3.10] modifies to:

$$\frac{\Psi'(x)}{\Psi(x)} = j\kappa(x) + \eta(x) \quad (3.11)$$

where  $\kappa(x) = \frac{m^*(x)R(x)}{2\hbar}$  and  $\eta(x) = \frac{m^*(x)X(x)}{2\hbar}$  are the propagation and attenuation constants of the wave function, respectively.

Integrating Eq.[3.11] from  $x = 0$  to any  $x$ ,  $\Psi(x)$  can be written as:

$$\Psi(x) = \Psi_0 e^{\int_0^x \eta(x) dx} e^{j \int_0^x \kappa(x) dx} \quad (3.12)$$

where  $\Psi(x)$  is the wave function at any point  $x$ . and  $\Psi_0$  is the incident wave function at the  $x = 0$  boundary.

### 3.3.2 Steady State Probability Current Density

The wave function,  $\Psi(x)$ , can be used to express the probability current density,  $J(x)$  as follows. Using Eq.[3.12], the steady state probability current density,  $J(x)$ , at any point  $x$  can be written in terms of  $R(x)$  and  $\eta(x)$  as:

$$J = \frac{1}{2} Re\left[\frac{2\hbar}{jm^*(x)} \Psi^*(x)\Phi(x)\right] = \frac{1}{2} |\Psi_0|^2 R(x) e^{2 \int_0^x \eta(x) dx} \quad (3.13)$$

where  $\Psi^*(x)$  is the complex conjugate of the wave function,  $\Psi(x)$ . At steady state, the current continuity equation necessitates that the probability current density everywhere along the barrier be equal in the absence of any generation or recombination mechanisms.

Using Eqs.[3.12] and [3.13],  $J(x)$  can be written as:

$$J = \frac{1}{2} R(x) |\Psi(x)|^2 \quad (3.14)$$

The current density,  $J(x)$ , can be defined in terms of an average steady state velocity,  $v_{av}(x)$ , and probability density as:

$$J = v_{av}(x) |\Psi(x)|^2 \quad (3.15)$$

This equation is similar to the drift current density equation in terms of the drift velocity, and charge density. Considering the probability current density again:

$$J(x) = \left(\frac{\hbar}{2jm^*(x)}\right) \left[\Psi^*(x) \frac{d\Psi(x)}{dx} - \frac{d\Psi^*(x)}{dx} \Psi(x)\right] \quad (3.16)$$

$J(x)$  can be modified to:

$$J(x) = \frac{1}{2} Re[\Phi(x)\Psi^*(x)] = \frac{1}{2} Re[V(x)I^*(x)] \quad (3.17)$$

Thus,  $J(x)$  is analogous to the average power in the transmission line.  $V(x)$  is the

voltage,  $I^*(x)$  is the complex conjugate of the current at any  $x$  along the transmission line.

### 3.3.3 Average Particle Traversal Time

Comparing Eqs.[3.14] and [3.15],  $v_{av}(x)$  can be written as :

$$v_{av}(x) = \frac{1}{2}R(x) \quad (3.18)$$

In other words, the average velocity of the particle at any  $x$  is one half the real part of the QMWI. The  $\tau_{APT}$  required for a particle to move an elemental distance,  $dx$ , at any point  $x$  is given by[3]:

$$d\tau_{APT} = \frac{dx}{v_{av}(x)} \quad (3.19)$$

Using Eqs.[3.16] and [3.19], an integral expression for the time required to traverse a distance  $L$  can be obtained as[3]:

$$\tau_{APT} = \int_0^L d\tau = 2 \int_0^L \frac{dx}{R(x)} \quad (3.20)$$

where  $R(x)$  is the real part of the Quantum Mechanical Wave Impedance,  $Z(x)$ . It is noted that using Eq.[3.10],  $Z(x)$  can be obtained from the wave function solution to the Schrödinger equation, given by Eq.[3.3]. Identifying the real part,  $R(x)$ , and using Eq.[3.20],  $\tau_{APT}$  can be obtained for any structure.

## Chapter 4

# SINGLE BARRIER

In this chapter, the APT time,  $\tau_{APT}$ , through a single rectangular potential barrier is considered. Based on the theoretical formulation, discussed in Chapter 3, an analytical expression for the  $\tau_{APT}$  is derived. In order to calculate the  $\tau_{APT}$  for the barrier region, the real part of the QMWI should be known. The real part of the quantum mechanical wave impedance can be obtained from the wave solution to the Schrödinger equation in that particular region. By knowing the real part of the QMWI, and using Eq.[3.20], an analytical expression for the  $\tau_{APT}$  is derived in terms of the incident energy, barrier height and width.

### 4.1 Calculation of the Complex Coefficients of Wave Function Solutions

The solutions to the time-independent Schrödinger equation for a rectangular potential barrier structure shown in Figure[4.1] is given by:

$$\Psi_1(x) = e^{ikx} + Ae^{-ikx} \dots\dots\dots x < \frac{-d}{2} \quad (4.1)$$

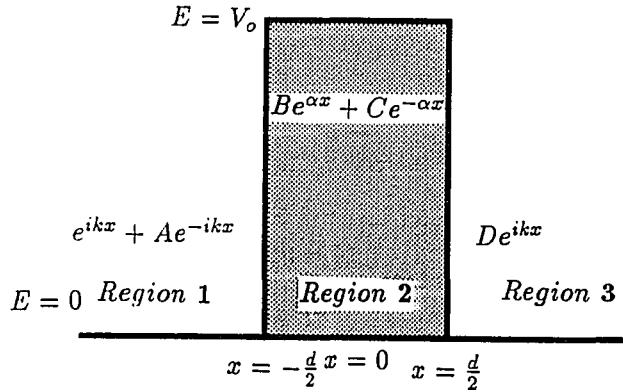


Figure 4.1: Conduction band edge profile for a single rectangular potential barrier with the corresponding wave function solution for different regions.

$$\Psi_2(x) = Be^{\alpha x} + Ce^{-\alpha x} \dots\dots\dots -\frac{d}{2} < x < \frac{d}{2} \quad (4.2)$$

$$\Psi_3(x) = De^{ikx} \dots\dots\dots x > \frac{d}{2} \quad (4.3)$$

where  $A$ ,  $B$ ,  $C$ , and  $D$  are the complex coefficients,  $\alpha$  is the attenuation constant given by  $\sqrt{\frac{2m^*(V_0-E)}{\hbar^2}}$ ,  $k$  is the propagation constant given by  $\sqrt{\frac{2m^*E}{\hbar^2}}$ ,  $V_0$  and  $d$  are the height and width of the potential barrier, respectively, and  $E$  is the incident energy of the particle.

### Boundary Conditions

The boundary conditions at  $x = -\frac{d}{2}$  and  $x = \frac{d}{2}$  are that the wave function,  $\Psi(x)$ , and the derivative of the wave function,  $\Psi'(x)$  be continuous, which are given by:

$$\Psi_1(x = -d/2) = \Psi_2(x = -d/2) \dots\dots\dots x = -\frac{d}{2} \quad (4.4)$$



$$\Psi_2(x = d/2) = \Psi_3(x = d/2) \dots \dots \dots x = \frac{d}{2} \quad (4.5)$$

$$\Psi'_1(x = -d/2) = \Psi'_2(x = -d/2) \dots \dots \dots x = -\frac{d}{2} \quad (4.6)$$

$$\Psi'_2(x = d/2) = \Psi'_3(x = d/2) \dots \dots \dots x = \frac{d}{2} \quad (4.7)$$

Substituting the respective wave function solutions from Eqs.[4.2] and [4.3] in Eqs.[4.4] - [4.7], at the interface  $x = \frac{d}{2}$ , an analytical expression for  $B$  and  $C$  can be obtained as:

$$B = \frac{De^{ikd/2}(\alpha + ik)}{2\alpha e^{\alpha d/2}} \quad (4.8)$$

$$C = \frac{De^{ikd/2}(\alpha - ik)}{2\alpha e^{-\alpha d/2}} \quad (4.9)$$

An expression for the complex coefficient  $A$  can be obtained by using the continuity condition on  $\Psi(x)$  and  $\Psi'(x)$  at the interface  $x = -\frac{d}{2}$  as follows:

$$e^{-ikd/2} + Ae^{ikd/2} = Be^{-\alpha d/2} + Ce^{\alpha d/2} \quad (4.10)$$

$$ike^{-ikd/2} - ikAe^{ikd/2} = \alpha Be^{-\alpha d/2} - \alpha Ce^{\alpha d/2} \quad (4.11)$$

Solving Eqs.[4.10] and [4.11] simultaneously and using Eqs.[4.8] and [4.9], the complex coefficient  $A$  can be obtained in terms of the the complex coefficient  $D$  as:

$$A = \frac{D(\alpha^2 + k^2) \sinh(\alpha d)}{i2k\alpha} \quad (4.12)$$

Using Eqs.[4.8],[4.9], and [4.12] in Eq.[4.10], an analytical expression for the complex constant  $D$  can be written as:

$$D = \frac{2ik\alpha e^{-ikd}}{(k^2 - \alpha^2) \sinh(\alpha d) + i2k\alpha \cosh(\alpha d)} \quad (4.13)$$

## 4.2 APT Time Expression for the Single Barrier

The solution to the Schrödinger equation in the potential barrier region is given by:

$$\Psi_2(x) = Be^{\alpha x} + Ce^{-\alpha x} \quad (4.14)$$

Reiterating the definition of Quantum Mechanical Wave Impedance (QMWI) given by Eq.[3.10]:

$$Z(x) = \frac{2\hbar}{jm^*} \frac{\Psi_2'(x)}{\Psi_2(x)} \quad (4.15)$$

Considering the fractional part of  $Z(x)$  and using Eq.[4.14] and [4.15], an analytical expression for  $\frac{\Psi_2'(x)}{\Psi_2(x)}$  can be obtained as:

$$\frac{\Psi_2'(x)}{\Psi_2(x)} = \frac{\alpha[Be^{\alpha x} - Ce^{-\alpha x}]}{[Be^{\alpha x} + Ce^{-\alpha x}]} \quad (4.16)$$

Substituting for  $B$  and  $C$  in terms of  $D$  from Eqs.[4.8] and [4.9] an expression for the QMWI can be written in terms of the attenuation constant  $\alpha$  and the propagation constant  $k$  as:

$$\frac{\Psi_2'(x)}{\Psi_2(x)} = \frac{\alpha[(\alpha + ik)e^{\alpha(x-d/2)} - (\alpha - ik)e^{-\alpha(x-d/2)}]}{[(\alpha + ik)e^{\alpha(x-d/2)} + (\alpha - ik)e^{-\alpha(x-d/2)}]} \quad (4.17)$$

Eq.[4.17] can be modified to:

$$\frac{\Psi_2'(x)}{\Psi_2(x)} = \frac{\alpha[\alpha \sinh(\alpha x') + ik \cosh(\alpha x')]}{[\alpha \cosh(\alpha x') + ik \sinh(\alpha x')]} \quad (4.18)$$

where  $x' = x - \frac{d}{2}$

Eq.[4.18] can also be written as:

$$\frac{\Psi_2'(x)}{\Psi_2(x)} = \frac{\alpha[(\alpha^2 + k^2) \sinh(\alpha x') \cosh(\alpha x') + ik\alpha]}{[\alpha^2 \cosh^2(\alpha x') + k^2 \sinh^2(\alpha x')]} \quad (4.19)$$

Multiplying by  $\frac{2\hbar}{jm^*}$ , the real part of  $Z(x)$ ,  $R(x)$ , can be obtained as:

$$Re[Z(x')] = \frac{2\hbar}{m^*} \left[ \frac{\alpha^2 k}{\alpha^2 \cosh^2(\alpha x') + k^2 \sinh^2(\alpha x')} \right] \quad (4.20)$$

The  $\tau_{APT}$  through the barrier can be obtained by substituting Eq.[4.20] into Eq.[3.20] as follows:

$$\tau_{APT} = 2 \int_{-d}^0 \left[ \frac{m^*}{2\hbar\alpha^2 k} \right] [\alpha^2 \cosh^2(\alpha x') + k^2 \sinh^2(\alpha x')] dx' \quad (4.21)$$

The above expression for  $\tau_{APT}$  is analytically integrable for all values of incident energy of the particle.

#### 4.2.1 The APT Time for $E < V_o$ .

When the energy of the incident electron,  $E$ , is less than the barrier height,  $V_o$ , the attenuation constant,  $\alpha$ , is a real quantity, and the electron wave function is decaying in nature. Then, Eq.[4.21] can be integrated to obtain  $\tau_{APT}$  given by:

$$\tau_{APT}^{below} = \left( \frac{m^*}{4\hbar\alpha^3 k} \right) [(k^2 + \alpha^2) \sinh(2\alpha d) + 2\alpha d(\alpha^2 - k^2)] \quad (4.22)$$

#### 4.2.2 The APT Time for $E > V_o$ .

When the energy of the incident electron,  $E$ , is more than the barrier height,  $V_o$ ,  $\alpha$  is an imaginary quantity, and the electron wave function is propagating in nature. Then Eq.[4.21] can be analytically integrated to obtain the following expression for  $\tau_{APT}$ :

$$\tau_{APT}^{above} = \left( \frac{m^*}{4\hbar k_B^3 k} \right) [2k_B d(k^2 + k_B^2) - (k^2 - k_B^2) \sin(2k_B d)] \quad (4.23)$$

where  $k_B$  is the propagation constant given by  $\sqrt{\frac{2m^*(E-V_o)}{\hbar^2}}$ .

### 4.3 Various energy limits of $\tau_{APT}$

The limiting values for the  $\tau_{APT}$  for three cases of the incident energy of the particle, *viz.*  $E \rightarrow 0$ ,  $E \rightarrow V_o$ , and  $E \rightarrow \infty$  can be computed analytically. The derivation of these limits are discussed in this section.

#### $E \rightarrow 0$ .

When the incident energy of the particle approaches zero,  $E \rightarrow 0$ , from Eq.[4.22] the propagation constant  $k$  tends to zero, hence  $\tau_{APT}$  given by Eq.[4.22], tends to the following limit:

$$\tau_{APT} \rightarrow \infty \quad (4.24)$$

#### $E \rightarrow \infty$ .

When the incident energy of the particle approaches infinity,  $E \rightarrow \infty$ , the propagation constant in the barrier,  $k_B \rightarrow \infty$ . The corresponding limit of  $\tau_{APT}$  is:

$$\tau_{APT} \rightarrow \frac{m^*}{4\hbar k_B^4} [2k_B d (2k_B^2)] \quad (4.25)$$

$$\tau_{APT} \rightarrow \frac{m^* d}{\hbar k_B} = \tau_{classical} \quad (4.26)$$

The  $\tau_{APT}$  tends to the classical time which is defined as the time it takes for a particle of same energy and effective mass to traverse a distance equal to the barrier width,  $d$ , in the absence of the barrier.

#### $E \rightarrow V_o$ .

When the incident energy,  $E$ , of the particle tends to the barrier height,  $V_o$ , the limiting values for the  $\tau_{APT}$  can be obtained from either Eqs.[4.22] or [4.23] as follows[19]:

$$\tau_{APT} \rightarrow \frac{m^*}{\hbar k \alpha^3} \left[ \frac{(k^2 + \alpha^2)}{4} [2\alpha d + \frac{(2\alpha d)^3}{6}] + \frac{(\alpha^2 - k^2)}{4} 2\alpha d \right] \quad (4.27)$$

$$\tau_{APT} \rightarrow \frac{m^*}{\hbar\alpha^3 k} \left[ \alpha^3 d + \frac{8\alpha^3 d^3}{6} \right] \quad (4.28)$$

$$\tau_{APT} \rightarrow \frac{m^* d}{\hbar k} \left[ 1 + \frac{(kd)^2}{3} \right] \quad (4.29)$$

From Eq.[4.29], the  $\tau_{APT}$  is finite when  $E \rightarrow V_o$  as  $k$  is finite. The limiting values of  $\tau_{dwell}$ ,  $\tau_{phase-delay}$ ,  $\tau_{B-L}$  and  $\tau_{classical}$  were obtained for three cases of limiting energies,  $E \rightarrow 0$ ,  $E \rightarrow \infty$  and  $E \rightarrow V_o$  and listed in Table I for comparison of these values. A detailed comparison is made in Chapter 6.

Table I. The limits for the traversal times; the dwell time,  $\tau_{dwell}$ , the phase-delay time,  $\tau_{phase-delay}$ , the Buttiker-Landauer time,  $\tau_{B-L}$ , the classical traversal time,  $\tau_{classical}$ , and the APT time,  $\tau_{APT}$ , for various incident energy limits.

	$E \rightarrow 0$	$E \rightarrow \infty$	$E \rightarrow V_o$
$\tau_{dwell}$	0	$\frac{m^* d}{\hbar k}$	$\frac{m^* k_o}{\hbar} \left( \frac{4d^3 + 6d/k_o^2}{12 + 3k_o^2 d^2} \right)$
$\tau_{phase-delay}$	$\infty$	$\frac{m^* d}{\hbar k}$	$\frac{m^* k_o}{\hbar} \left( \frac{4d^3 + 6d/k_o^2}{12 + 3k_o^2 d^2} \right)$
$\tau_{B-L}$	$\left( \frac{m^* k_o^2}{\hbar \alpha^2} \right) \frac{(\alpha^2 - k^2) \sinh^2(\alpha d) + (\alpha d k_o^2 / 2) \sinh(2\alpha d)}{4k^2 \alpha^2 + k_o^2 \sinh^2(\alpha d)}$	$\frac{m^* d}{\hbar k}$	$\sqrt{\tau_x^2 + \tau_y^2}^\ddagger$
$\tau_{classical}$	$\infty$	$\frac{m^* d}{\hbar k}$	$\frac{m^* d}{\hbar k}$
$\tau_{APT}$	$\infty$	$\frac{m^* d}{\hbar k}$	$\frac{m^* d}{\hbar k} \left[ 1 + \frac{(kd)^2}{3} \right]$

$\ddagger \tau_x = \left( \frac{m^*}{\hbar} \right) \left( \frac{3d^2 + 2d^4 k_o^2}{12 + 3k_o^2 d^2} \right)$  and  $\tau_y = \left( \frac{m^* k_o}{\hbar} \right) \left( \frac{4d^3 + 6d/k_o^2}{12 + 3k_o^2 d^2} \right)$

## Chapter 5

# DOUBLE BARRIER

In this chapter, an analytical expression for the  $\tau_{APT}$  through a symmetrical double rectangular potential barrier structure is obtained by using an approach similar to that used for a single barrier case in Chapter 4.

The conduction band edge profile of a symmetrical double rectangular potential barrier is shown in Figure [5.1]. Firstly, the solution to the Schrödinger equation is obtained analytically. Then the solution is used to obtain the real part of the QMWI, which in turn is used to obtain  $\nu_{av}(x)$ .  $\nu_{av}(x)$  is used to obtain an analytical expression for the  $\tau_{APT}$ .

### 5.1 Calculation of the Complex Coefficients of Wave Function Solutions

The wave function solution to Schrödinger equation in the five regions shown in Figure[5.1] is given by:

$$\Psi_1(x) = e^{ikx} + Ae^{-ikx} \dots\dots\dots x < 0 \quad (5.1)$$

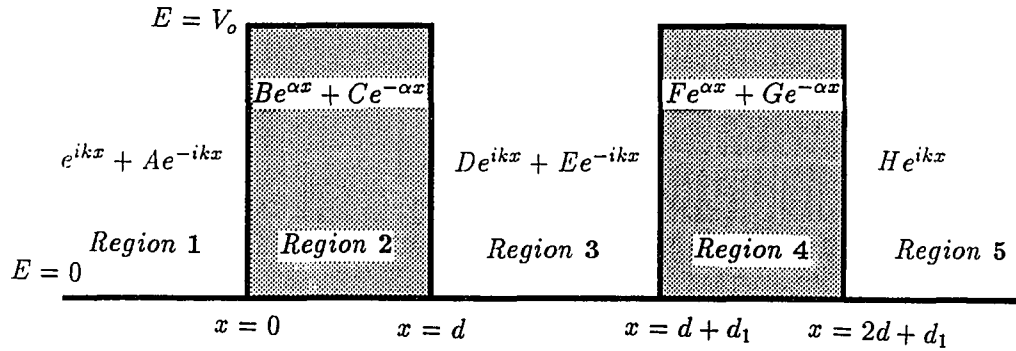


Figure 5.1: Conduction band edge profile for a symmetrical double rectangular potential barrier with the wave function solutions for different regions.

$$\Psi_2(x) = Be^{\alpha x} + Ce^{-\alpha x} \dots\dots\dots 0 < x < d \quad (5.2)$$

$$\Psi_3(x) = De^{ikx} + Ee^{-ikx} \dots\dots\dots d < x < (d + d_1) \quad (5.3)$$

$$\Psi_4(x) = Fe^{\alpha x} + Ge^{-\alpha x} \dots\dots\dots (d + d_1) < x < (d_1 + 2d) \quad (5.4)$$

$$\Psi_5(x) = He^{ikx} \dots\dots\dots x > (d_1 + 2d) \quad (5.5)$$

where  $d$  and  $d_1$  are the barrier and well widths, respectively, and  $V_0$  is the height of the barrier. Applying the boundary conditions *viz.* the wave function,  $\Psi(x)$ , and the derivative of the wave function,  $\Psi'(x)$ , are continuous at the interfaces  $x = 0$ ,  $x = d$ ,  $x = d + d_1$ , and at  $x = 2d + d_1$ , analytical expressions for the complex coefficients A, B, C, D, E, F, and G, can be obtained in

terms of the complex constant  $H$ , which is the wave function transmission coefficient. The analytical solutions to the complex coefficients are:

$$A = \frac{e^{i2kd}}{i2k\alpha e^{\alpha d}} \left( \frac{\alpha + ik}{\alpha - ik} \right) [ [(k^2 - \alpha^2) + (\alpha - ik)^2 e^{i2kd_1}] \sinh(\alpha d) + i2k\alpha \cosh(\alpha d) ] - \left( \frac{\alpha + ik}{\alpha - ik} \right) \quad (5.6)$$

$$B = \frac{H e^{ik2d} (\alpha + ik)}{i4k\alpha^2 e^{\alpha d}} [ [(k^2 - \alpha^2) + e^{i2kd_1} (\alpha - ik)^2] \sinh(\alpha d) + i2k\alpha \cosh(\alpha d) ] \quad (5.7)$$

$$C = \frac{H e^{i2kd} (\alpha - ik)}{i4k\alpha^2 e^{-\alpha d}} [ [(k^2 - \alpha^2) + e^{i2kd_1} (\alpha + ik)^2] \sinh(\alpha d) + i2k\alpha \cosh(\alpha d) ] \quad (5.8)$$

$$D = \frac{H e^{ikd}}{i2k\alpha} [(k^2 - \alpha^2) \sinh(\alpha d) + i2k\alpha \cosh(\alpha d)] \quad (5.9)$$

$$E = \frac{H e^{ik(3d+2d_1)}}{i2k\alpha} (\alpha^2 + k^2) \sinh(\alpha d) \quad (5.10)$$

$$F = \frac{H e^{ik(2d+d_1)} (\alpha + ik)}{2\alpha e^{\alpha(2d+d_1)}} \quad (5.11)$$

$$G = \frac{H e^{ik(2d+d_1)} (\alpha - ik)}{2\alpha e^{-\alpha(2d+d_1)}} \quad (5.12)$$

## 5.2 The $\tau_{APT}$ for a Resonant Tunneling Structure

In order to derive an analytical expression for the  $\tau_{APT}$ , the Quantum Mechanical Wave Impedance (QMWI) should be computed. The QMWI can be obtained from the wave function solution involving the complex constants  $B$ ,  $C$ ,  $D$ ,  $E$ ,  $F$ , and  $G$ . The analytical expressions for the real and imaginary parts of the complex coefficients are given in Appendix A. The real parts are subscripted '1' and the



imaginary parts are subscripted '2'. In order to calculate the total  $\tau_{APT}$  through the structure, the  $\tau_{APT}$ 's for the two barriers and the well region are calculated individually and added up as follows:

$$\tau_{APT}^{total} = \tau_{APT}^{lb} + \tau_{APT}^{well} + \tau_{APT}^{rb} \quad (5.13)$$

where  $\tau_{APT}^{lb}$ ,  $\tau_{APT}^{well}$ , and  $\tau_{APT}^{rb}$  are the traversal times in the left barrier region, well region, and right barrier region, respectively. The  $\tau_{APT}$ 's,  $\tau_{APT}^{lb}$ ,  $\tau_{APT}^{well}$  and  $\tau_{APT}^{rb}$  are calculated using the integral expression for  $\tau_{APT}$  given by Eq.[3.20].

### 5.2.1 The $\tau_{APT}$ for the Left Barrier Region

In order to calculate the  $\tau_{APT}$  time for the barrier region, the real part of the QMWI should be computed. Once the the real part of the QMWI,  $Re[Z(x)]$ , is known, it can be substituted into Eq.[3.20] to obtain an integral expression for the  $\tau_{APT}$  for the barrier region.

The solution to the time-independent Schrödinger equation for the left barrier region is given by:

$$\Psi(x) = (B_1 + iB_2)e^{\alpha x} + (C_1 + iC_2)e^{-\alpha x} \quad (5.14)$$

where  $B_1, C_1$  are the real parts and  $B_2, C_2$  are the imaginary parts of the complex constants  $B$  and  $C$ , respectively. The  $\Psi'(x)$  can be obtained from Eq.[5.14] as:

$$\Psi'(x) = \alpha[(B_1 + iB_2)e^{\alpha x} - (C_1 + iC_2)e^{-\alpha x}] \quad (5.15)$$

$Re[Z(x)]$  can be obtained from Eq.[5.14], Eq.[5.15] and Eq.[3.19] as:

$$Re[Z(x)] = \left(\frac{2\hbar\alpha}{m^*}\right) \left[ \frac{2(B_2C_1 - B_1C_2)}{(B_1^2 + B_2^2)e^{2\alpha x} + (C_1^2 + C_2^2)e^{-2\alpha x} + 2(B_1C_1 + B_2C_2)} \right] \quad (5.16)$$

$\tau_{APT}^{lb}$  can be obtained from Eq.[5.16] and Eq.[3.20] as:

$$\tau_{APT}^{lb} = 2 \int_0^d \left( \frac{m^* dx}{2\hbar\alpha} \right) \left[ \frac{(B_1^2 + B_2^2)e^{2\alpha x} + (C_1^2 + C_2^2)e^{-2\alpha x} + 2(B_1C_1 + B_2C_2)}{2(B_2C_1 - B_1C_2)} \right] \quad (5.17)$$

Integrating Eq.[5.17]:

$$\tau_{APT}^{lb} = \left[ \frac{m^*}{4\hbar\alpha(B_2C_1 - B_1C_2)} \right] \left[ \left( \frac{B_1^2 + B_2^2}{2\alpha} \right) [e^{2\alpha d} - 1] - \left( \frac{C_1^2 + C_2^2}{2\alpha} \right) [e^{-2\alpha d} - 1] + 2d(B_1C_1 + B_2C_2) \right] \quad (5.18)$$

### 5.2.2 The $\tau_{APT}$ for the Potential Well Region

The solution to the time-independent Schrödinger equation for the well region is given by:

$$\Psi(x) = (D_1 + iD_2)e^{ikx} + (E_1 + iE_2)e^{-ikx} \quad (5.19)$$

where  $D_1, E_1$  are the real parts and  $D_2, E_2$  are the imaginary parts of the complex constants  $D$  and  $E$ , respectively. The expressions for all the coefficients are given in appendix A. The  $\Psi'(x)$  is obtained from Eq.[5.19] as:

$$\Psi'(x) = ik[(D_1 + iD_2)e^{ikx} - (E_1 + iE_2)e^{-ikx}] \quad (5.20)$$

The  $\tau_{APT}$  in the potential well region can be written as:

$$\tau_{APT}^{well} = 2 \int_d^{d+d_1} \frac{dx}{Re[Z(x)]} \quad (5.21)$$

Using Eq.[5.19] and Eq.[5.20] in Eq.[3.9], and writing the exponentials in terms of trigonometric functions, multiplying by  $\frac{2\hbar}{m^*}$ , in the expression for  $Re[Z(x)]$  in terms of the complex coefficients, an expression for the  $\tau_{APT}$  for the well region can be obtained as:

$$\tau_{APT}^{well} = \int_d^{d+d_1} [p + q \cos(2kx) + r \sin(2kx)] dx \quad (5.22)$$

where  $p$ ,  $q$ , and  $r$  are given by:

$$p = \frac{D_1^2 + D_2^2 + E_1^2 + E_2^2}{D_1^2 + D_2^2 - E_1^2 - E_2^2} \quad (5.23)$$

$$q = \frac{D_1 E_1 + D_2 E_2}{D_1^2 + D_2^2 - E_1^2 - E_2^2} \quad (5.24)$$

$$r = \frac{D_1 E_2 - D_2 E_1}{D_1^2 + D_2^2 - E_1^2 - E_2^2} \quad (5.25)$$

Integrating Eq.[5.22], an analytical expression for the  $\tau_{APT}$  in the well region,  $\tau_{APT}^{well}$ , is obtained as follows:

$$\tau_{APT}^{well} = \left(\frac{m^*}{2\hbar k}\right) [pd_1 + \left(\frac{q}{2k}\right) [\sin[2k(d+d_1)] - \sin(2kd)] - \left(\frac{r}{2k}\right) [\cos[2k(d+d_1)] - \cos(2kd)]] \quad (5.26)$$

### 5.2.3 The $\tau_{APT}$ for the Right Barrier Region

The solution to the time-independent Schrödinger equation in the barrier region is given by:

$$\Psi(x) = (F_1 + iF_2)e^{\alpha x} + (G_1 + iG_2)e^{-\alpha x} \quad (5.27)$$

where  $F_1$ ,  $G_1$  are the real parts and  $F_2$ ,  $G_2$  are the imaginary parts of the complex constants  $F$  and  $G$ , respectively.  $\Psi'(x)$  can be obtained from Eq.[5.27] as:

$$\Psi'(x) = \alpha[(F_1 + iF_2)e^{\alpha x} - (G_1 + iG_2)e^{-\alpha x}] \quad (5.28)$$

$Re[Z(x)]$  can be obtained from Eq.[5.27] and Eq.[5.28] as follows:

$$Re[Z(x)] = \left( \frac{2\hbar\alpha}{m^*} \right) \left[ \frac{2(F_2G_1 - F_1G_2)}{(F_1^2 + F_2^2)e^{2\alpha x} + (G_1^2 + G_2^2)e^{-2\alpha x} + 2(F_1G_1 + F_2G_2)} \right] \quad (5.29)$$

and the  $\tau_{APT}^{rb}$  can be obtained as follows:

$$\tau_{APT}^{rb} = 2 \int_{d+d_1}^{2d+d_1} \left( \frac{m^* dx}{2\hbar\alpha} \right) \left[ \frac{(F_1^2 + F_2^2)e^{2\alpha x} + (G_1^2 + G_2^2)e^{-2\alpha x} + 2(F_1G_1 + F_2G_2)}{2(F_2G_1 - F_1G_2)} \right] \quad (5.30)$$

Integrating Eq.[5.30]:

$$\begin{aligned} \tau_{APT}^{rb} &= \left[ \frac{m^*}{4\hbar\alpha(F_2G_1 - F_1G_2)} \right] \\ &\quad \left[ \left[ \frac{F_1^2 + F_2^2}{2\alpha} \right] [e^{2\alpha(d_1+2d)} - e^{2\alpha(d_1+d)}] - \left[ \frac{G_1^2 + G_2^2}{2\alpha} \right] \right. \\ &\quad \left. [e^{-2\alpha(d_1+2d)} - e^{-2\alpha(d_1+d)}] + 2d(F_1G_1 + F_2G_2) \right] \end{aligned} \quad (5.31)$$

## Chapter 6

# RESULTS, COMPARISONS and DISCUSSIONS

In this chapter, the  $\tau_{APT}$  obtained from the analytical expressions are compared with previous work reported in the literature for the single and double barrier cases. The  $\tau_{APT}$  for single barrier is compared with the dwell time[7, 45], the phase-delay time[7, 16, 26, 50], the Buttiker-Landauer traversal time[7, 8, 9], and the classical traversal time. The double barrier  $\tau_{APT}$  is compared with the experimentally obtained maximum frequency of oscillation of some of the structures experimentally grown and tested by Sollner *et. al.* [25, 47, 48].

### 6.1 Single Barrier

A plot of  $\tau_{APT}$  and transmission coefficient vs. the normalized incident energy for a rectangular potential barrier is shown in Figure[6.2] for a barrier of height  $0.3eV$  and width of  $200\text{\AA}$  as shown in Figure[6.1], for the case of incident energy of the particle less than the barrier height, i.e.,  $E < V_o$ . The transmission coefficient increases with incident energy,  $E$ , as expected. The  $\tau_{APT}$  decreases with increasing energy. It is noted that the  $\tau_{APT}$  reaches infinity in the limit of zero energy like a classical

particle. A plot of  $\tau_{APT}$  and transmission coefficient vs. the normalized incident energy is shown in Figure[6.3] for the structure shown in Figure[6.1], where the incident energy of the particle is more than the barrier height, i.e.,  $E > V_o$ . In the limit of incident energy of the particle tending to the barrier height, i.e.  $E \rightarrow V_o$ , the  $\tau_{APT}$  is large but finite as given by Eq.[4.29]. The  $\tau_{APT}$  decreases with the increasing incident energy. It is also noted that the  $\tau_{APT}$  oscillates slightly for large barrier thicknesses. In the limit of  $E \rightarrow \infty$ ,  $\tau_{APT}$  reaches the classical limit as given by Eq.[4.26].

### 6.1.1 Comparison of Dwell time, Phase-delay time, Buttiker-Landauer time, $\tau_{APT}$ , and the Classical time for, $E < V_o$

A plot of the dwell time, the phase-delay time, the Buttiker-Landauer time, the  $\tau_{APT}$  and the classical traversal time vs. normalized incident energy is shown in Figure[6.4], for a rectangular potential barrier with a barrier height of  $0.3eV$  and a width of  $200\text{\AA}$  as shown in Figure[6.1], when  $E < V_o$ .

$\tau_{APT}$  is always greater than the classical time.  $\tau_{APT}$  is infinity in the limit of no energy,  $E = 0$ , implying that the particle takes infinite time to traverse the distance when the particles possess no energy at all. For all incident energy values below the barrier height,  $V_o$ , the dwell time and the phase-delay time are less than the classical traversal time as shown in Figure[6.4]. Whereas, the Buttiker-Landauer time is below the classical time for a range of incident energy, and above the classical time for the rest of the incident energy interval.

### 6.1.2 Comparison of Dwell time, Phase-delay time, Buttiker-Landauer time, $\tau_{APT}$ , and the Classical time for $E > V_o$

A plot of the dwell time, the phase-delay time, the Buttiker-Landauer time, the  $\tau_{APT}$  and the classical traversal time vs. normalized incident energy are shown in Figure[6.5], for a rectangular potential barrier with a barrier height of  $0.3eV$  and a width of  $200\text{\AA}$  as shown in Figure[6.1], when  $E > V_o$ . In this case, all the traversal times are above the classical traversal time. A plot of the

dwel time, the phase-delay time, the Buttiker-Landauer time, the  $\tau_{APT}$ , and the classical time with the transmission coefficient is shown in Figure[6.6]. The dwell time, the phase-delay time and the Buttiker-Landauer time attain a maximum value when the transmission coefficient is maximum, and reaches a minimum when the transmission is minimum. Whereas, the  $\tau_{APT}$  attains a minimum when the transmission coefficient is maximum, and reaches a maximum when transmission is minimum. In other words, According to  $\tau_{APT}$ , the particle travels fastest at resonant energies, whereas according to the approaches, the particle travels fastest at non-resonant energies. All the traversal times approach the classical time limit at very high incident energies.

### 6.1.3 Effect of the barrier width on the $\tau_{APT}$

The dependence of  $\tau_{APT}$  on the barrier width with  $E < V_0$  is shown in Figure[6.7], for a barrier height of  $1.0eV$  and for a barrier width in the range of  $25\text{\AA}$  to  $250\text{\AA}$ .

The  $\tau_{APT}$  decreases as the incident energy of the particle increases and the  $\tau_{APT}$  is inversely related to the transmission coefficient. The  $\tau_{APT}$  is finite when the incident energy of the particle is equal to the barrier height  $V_0$ .

The dependence of  $\tau_{APT}$  on barrier width, with incident energy of the particle more than the barrier height is shown in Figure[6.8], for a barrier height of  $1.0eV$  and for a barrier width in the range from  $25\text{\AA}$  to  $250\text{\AA}$ . Small oscillations in the  $\tau_{APT}$  can be seen as the width of the potential barrier increases.

The  $\tau_{APT}$  decreases as the incident energy of the particle increases. It is to be noted that as the barrier thickness increases, small oscillations in the  $\tau_{APT}$  can be observed. These oscillations are inversely proportional to the transmission coefficient. i.e.  $\tau_{APT}$  valleys at resonant energies whereas the transmission coefficient peaks.

## 6.2 Double Barrier

The plot of the transmission coefficient and  $\tau_{APT}$  is shown in Figure[6.10] for the structure shown in Figure[6.9]. Five quasi-bound energy states can be observed below the barrier height. The transmission coefficient is unity at these resonant energies levels. It is to be noted that  $\tau_{APT}$  is minimum at the resonant energies. Thus the transmission coefficient is inversely related to  $\tau_{APT}$ .

### 6.2.1 Comparison of $\tau_{APT}$ with Experimental Results

**Structure 1: Barrier width =  $50\text{\AA}$ , Well width =  $50\text{\AA}$ , and Barrier height =  $0.23eV$ .**

The plot of  $\tau_{APT}$  and the transmission coefficient vs. the incident energy of the particle is shown in Figure[6.12]. The structure considered was a symmetrical rectangular double potential barrier with a barrier height of  $0.23eV$ , barrier width of  $50\text{\AA}$  and a well width of  $50\text{\AA}$  as shown in Figure [6.11]. This same structure is chosen as it is well characterized experimentally in terms of the  $I - V$  characteristics and high frequency studies[47, 48]. It was reported by Sollner *et. al.*[47, 48] that the maximum frequency of operation of the resonant tunneling device is  $1.2THz$ . It was also observed that there is one quasi-bound resonant energy state at  $0.0791eV$  which is less than the barrier height. This value of  $0.0791eV$  agrees with that obtained from our analytical solutions. At this resonant energy value, the  $\tau_{APT}$  is a minimum and also the transmission coefficient attains unity. The estimated maximum frequency of operation, from analytical expression for  $\tau_{APT}$ , is  $0.8THz$ , i.e., frequency corresponding to the resonant energy, which is in good agreement with the experimental value of  $1.2THz$ . This maximum frequency of operation was estimated taking into consideration only the  $\tau_{APT}$ . The capacitance charging times at the depletion layers are not taken into consideration.



**Structure 2: Barrier width =  $25\text{\AA}$ , Well width =  $45\text{\AA}$ , and Barrier height =  $1.0eV$ .**

The plot of  $\tau_{APT}$  and the transmission coefficient vs. the incident energy of the particle is shown in Figure[6.14]. The structure considered was a symmetrical rectangular double potential barrier with a barrier height of  $1.0eV$ , barrier width of  $25\text{\AA}$  and a well width of  $45\text{\AA}$  as shown in Figure [6.13]. This structure was fabricated and experimentally studied for high frequency oscillations by Sollner *et. al.*[25, 47]. It was reported by Sollner *et. al.*, that the maximum frequency of operation of the above resonant tunneling device is  $2.4THz$ . It was also reported that there are two quasi-bound resonant energy states, one at  $0.154eV$  and the other at  $0.581eV$  below the barrier height. These values agree well with the values obtained from other numerical solutions. The transmission coefficient is maximum and attains the value of unity at these resonant energy levels and  $\tau_{APT}$  at these resonant energy levels is a minimum. The estimated maximum frequency of operation is  $1.4THz$  which is in good agreement with the experimental results. The maximum frequency of operation was estimated by taking into consideration the  $\tau_{APT}$  only.

### 6.2.2 Effect of barrier width on the APT time

A 3-dimensional surface plot of the  $\tau_{APT}$  is shown in Figure[6.16], for a range of the barrier widths from  $30\text{\AA}$  to  $100\text{\AA}$ , well width of  $30\text{\AA}$ , and for a barrier height of  $0.3eV$ , as shown in Figure[6.15]. The  $\tau_{APT}$  approaches infinity when  $E \rightarrow 0$ . The  $\tau_{APT}$  is inversely related to the transmission coefficient. The formation of troughs in the  $\tau_{APT}$  at resonances indicate that at these resonant energy levels, the  $\tau_{APT}$  is minimum. As the barrier thickness is increased, the formation of the resonant energy levels is more pronounced and  $\tau_{APT}$  for a very thick barrier, at the resonance, is more than that for a thin barrier.

### 6.2.3 Effect of well width on the APT time

A 3-dimensional surface plot of the  $\tau_{APT}$  is shown in Figure[6.18], for a range of well widths from  $30\text{\AA}$  to  $110\text{\AA}$  and a barrier width of  $30\text{\AA}$ , and for a barrier height of  $1.0eV$  as shown in Figure[6.17]. A 3-dimensional surface plot of the  $\tau_{APT}$  along with the transmission coefficient is shown in Figure[6.19] for the same structure shown in Figure[6.17]. More quasi-bound states with  $E < V_o$  appear as the well width increases, as shown in Figures[6.18] and [6.19]. The formation of troughs in the  $\tau_{APT}$  at resonances indicate that at these resonant energy levels, the  $\tau_{APT}$  is minimum.  $\tau_{APT}$  is minimum at resonant energies. When the width of the potential well is small, the number of resonant energies is small within the potential well. As the width of the potential well increases, the number of resonant energy levels increase and the energy spacing between any two adjacent resonant energy levels within the potential well,  $\Delta E$ , decreases.

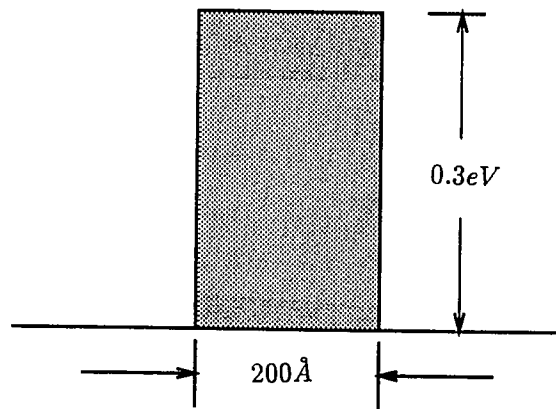


Figure 6.1: The conduction band edge profile of a single rectangular potential barrier of width  $200\text{\AA}$  and height  $0.3\text{eV}$

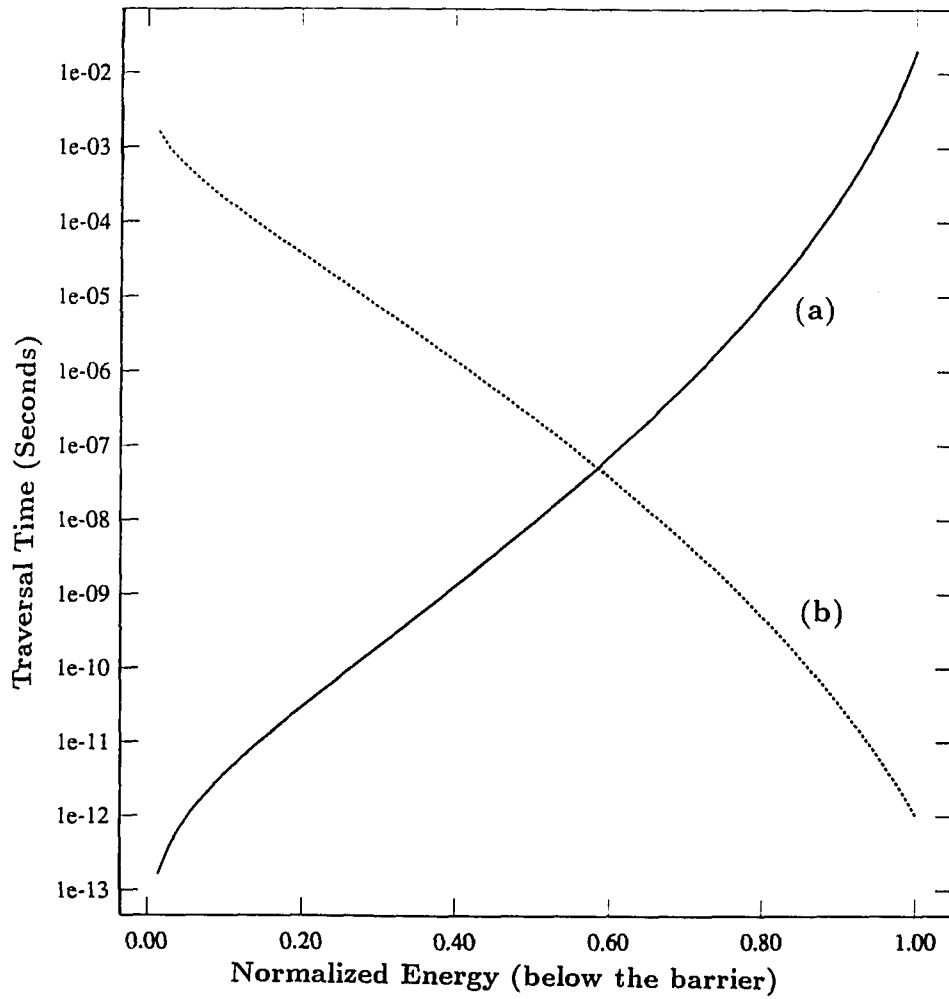


Figure 6.2: Plot of the (a) Transmission Coefficient, and the (b) APT time, for a single rectangular potential barrier for  $E < V_0$ , with barrier width  $200\text{\AA}$  and barrier height  $0.3eV$

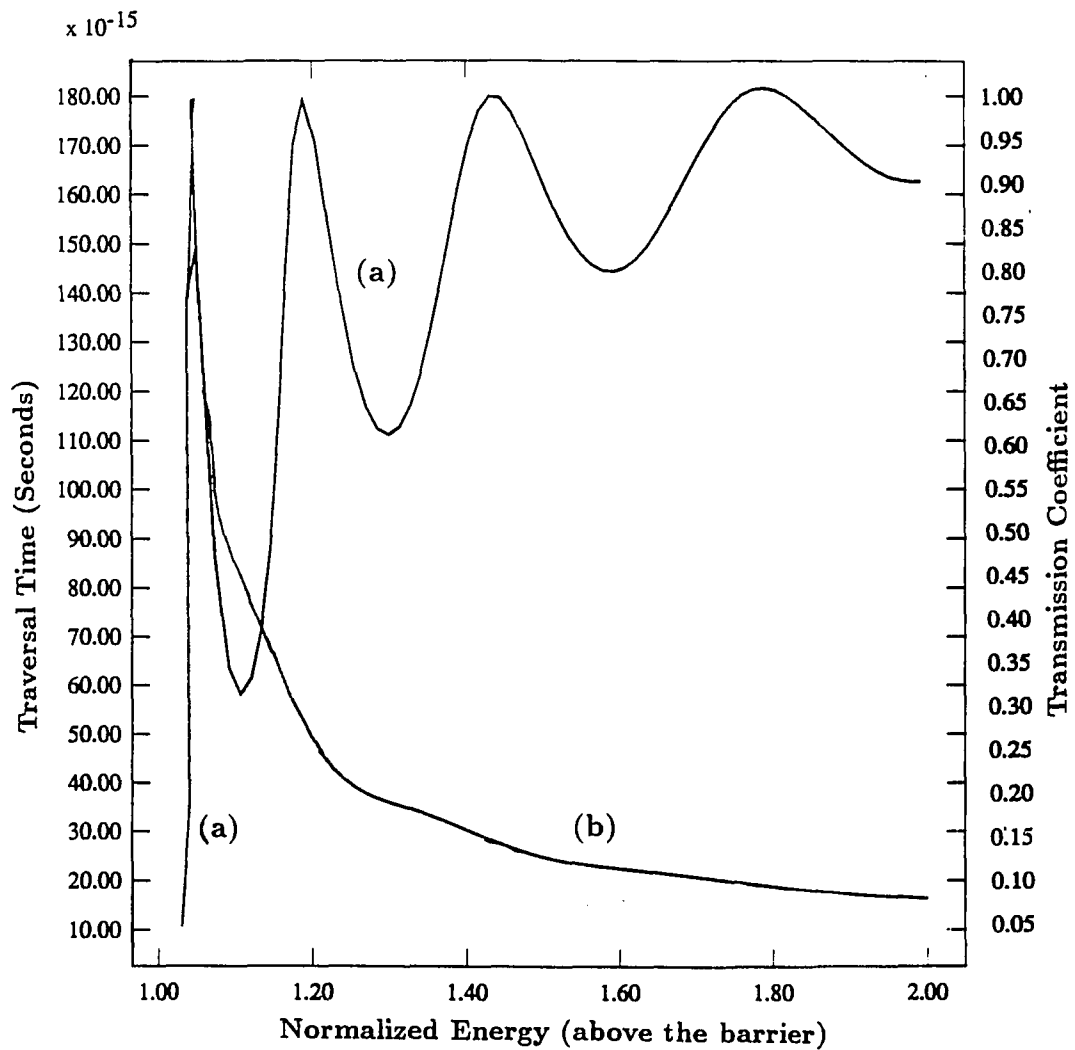


Figure 6.3: Plot of the (a) Transmission Coefficient, and the (b) APT time, for a single rectangular potential barrier for  $E > V_0$ , with barrier width  $200\text{\AA}$  and barrier height  $0.3\text{eV}$

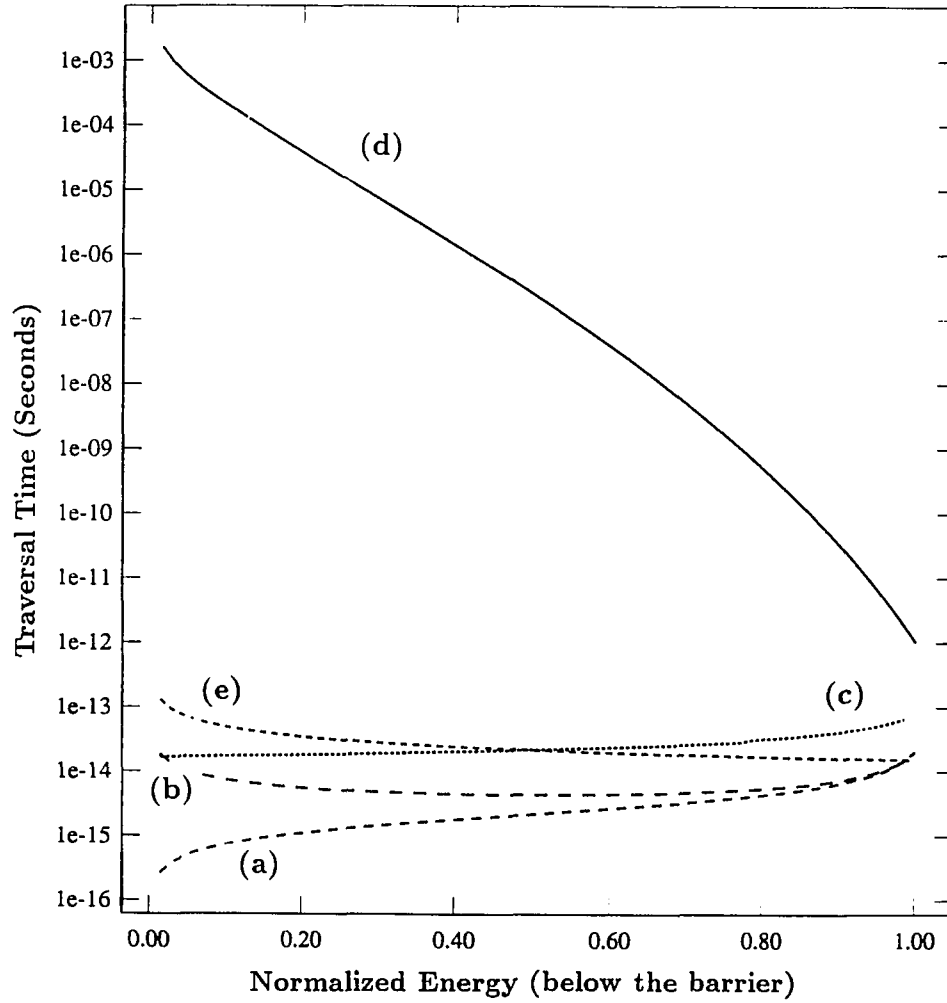


Figure 6.4: Plot of the Traversal Times : (a) Dwell Time, (b) Phase-Delay Time, (c) Buttiker-Landauer Time, (d) APT time, and (e) Classical Time for  $E < V_0$ , with barrier width  $200\text{\AA}$  and barrier height  $0.3\text{eV}$ .

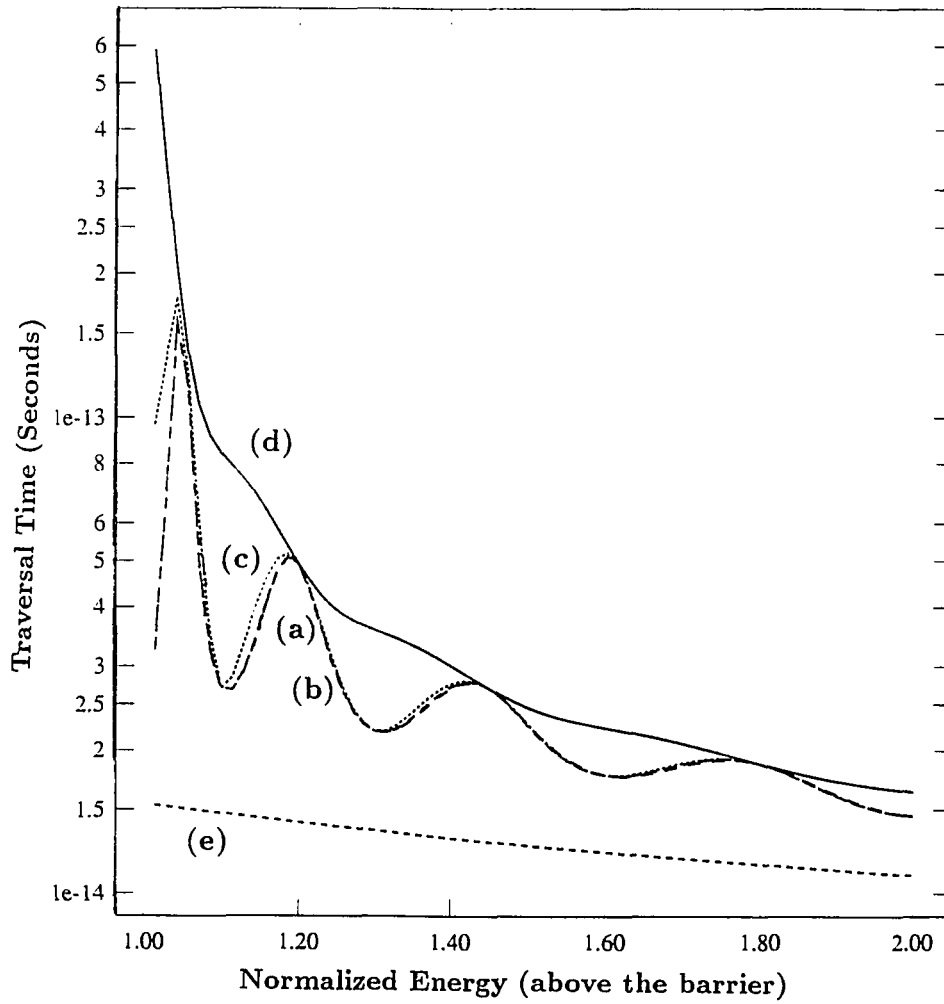


Figure 6.5: Plot of the Traversal Times : (a) Dwell Time, (b) Phase-Delay Time, (c) Buttiker-Landauer Time, (d) APT time, and (e) Classical Time for  $E > V_o$ , with barrier width  $200\text{\AA}$  and barrier height  $0.3eV$ .

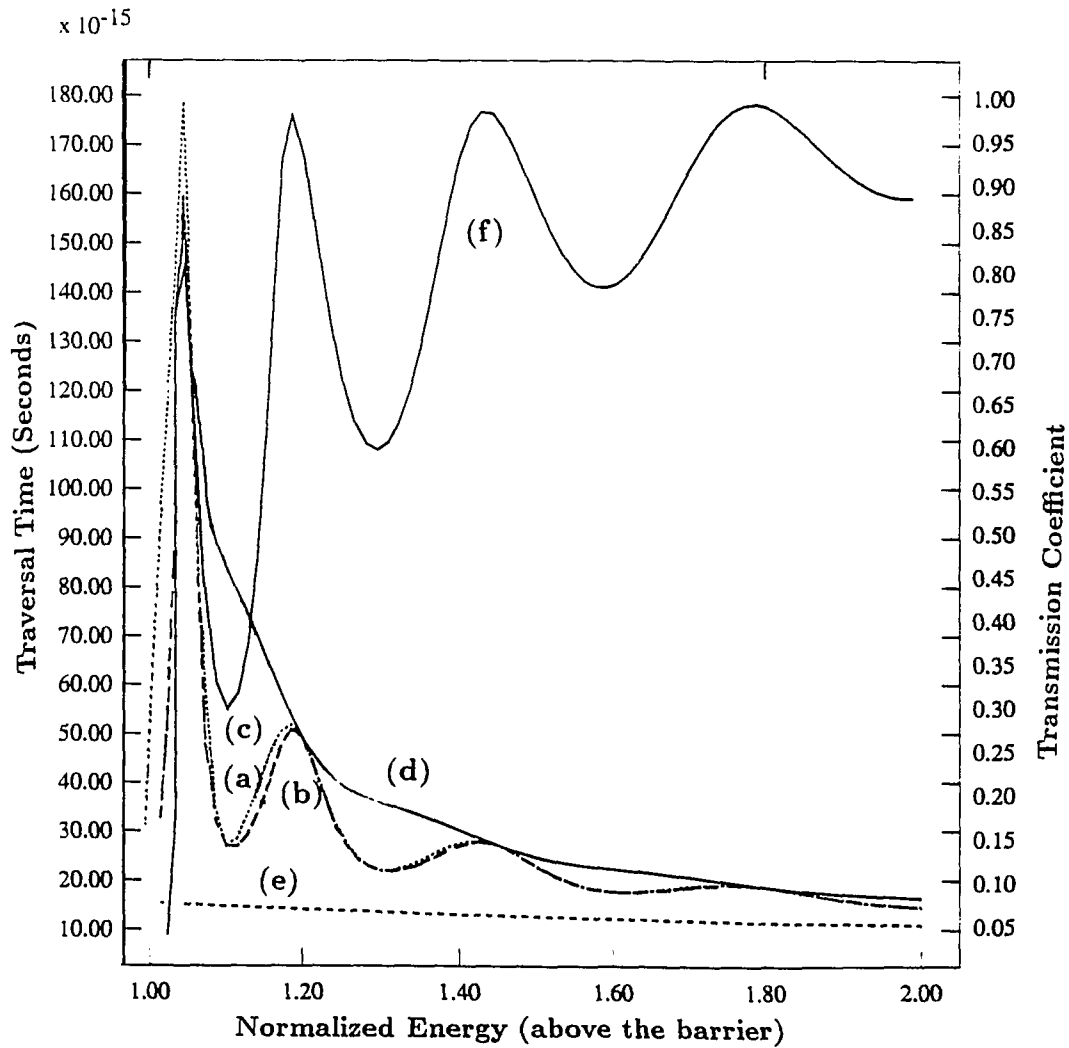


Figure 6.6: Plot of the Traversal Times : (a) Dwell Time, (b) Phase-Delay Time, (c) Buttiker-Landauer Time, (d) APT time, (e) Classical Time, and the (f) Transmission Coefficient for  $E > V_0$ , with barrier width  $200\text{\AA}$  and barrier height  $0.3eV$ .



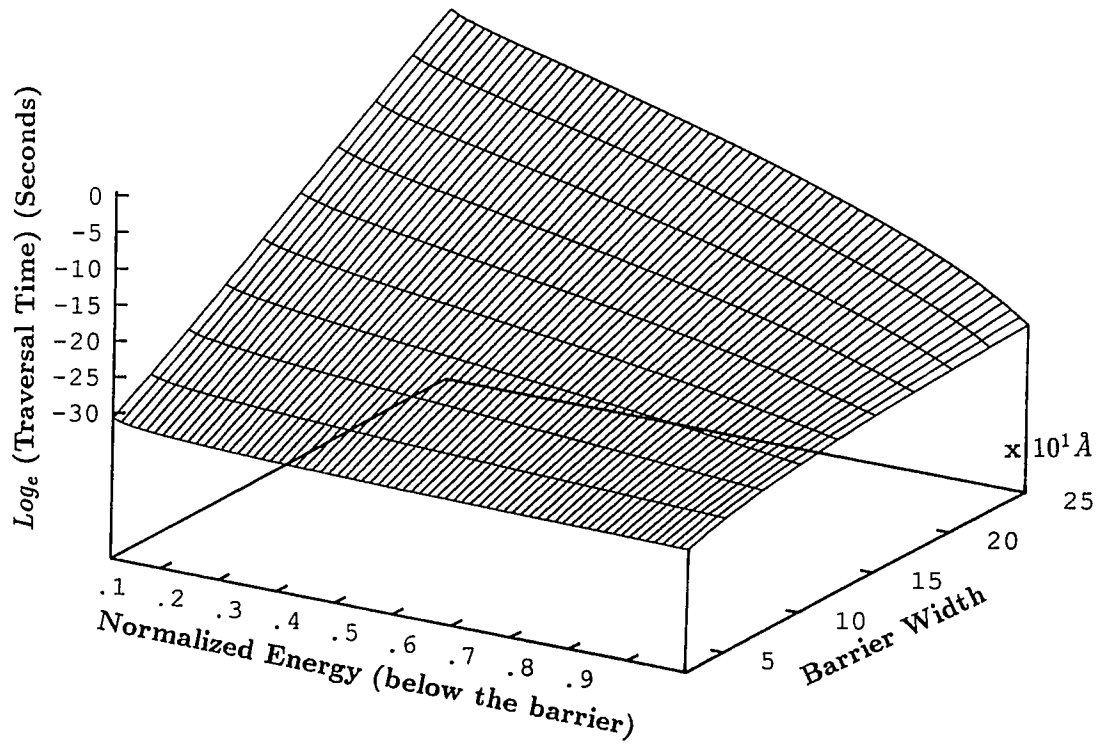


Figure 6.7: 3-Dimensional surface plot of the APT time, for the case of  $E < V_0$  with the barrier height  $1.0\text{eV}$  and barrier width in the range  $25\text{\AA}$  to  $250\text{\AA}$ .

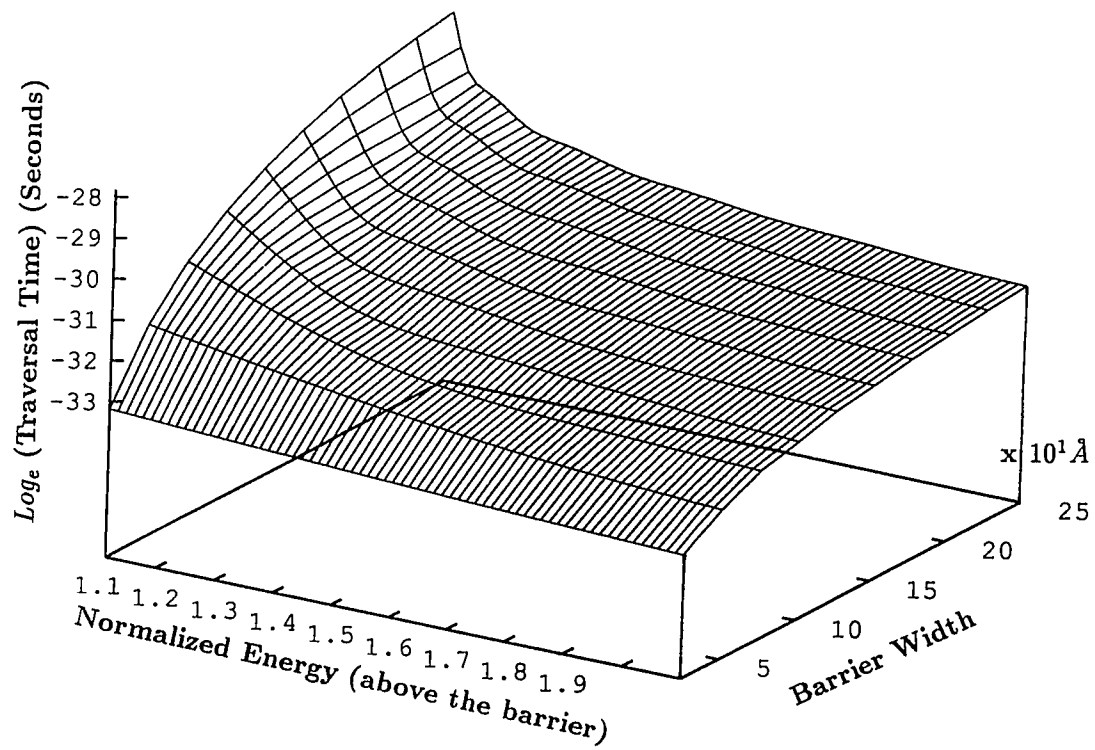


Figure 6.8: 3-Dimensional surface plot of the APT time, for the case of  $E > V_0$  with the barrier height  $1.0\text{eV}$  and barrier width in the range  $25\text{\AA}$  to  $250\text{\AA}$ .

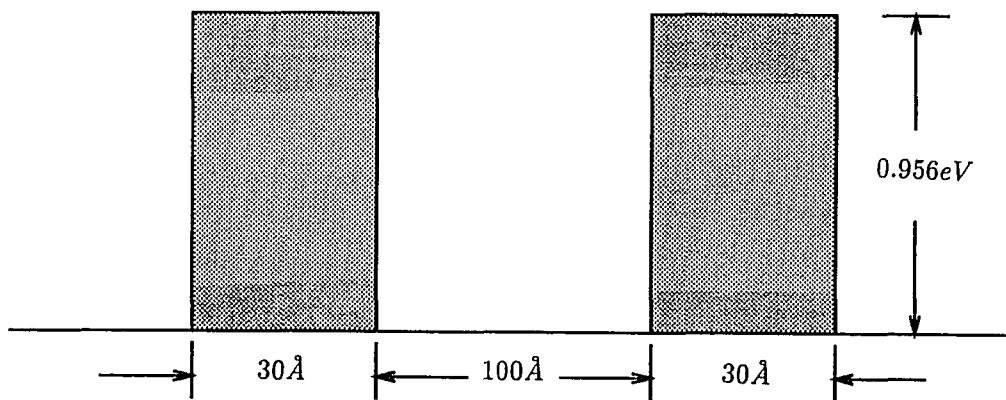


Figure 6.9: The conduction band edge profile of a symmetrical double rectangular potential barrier structure with a barrier height of  $0.956\text{eV}$ , barrier width of  $30\text{\AA}$  and a well width of  $100\text{\AA}$ .

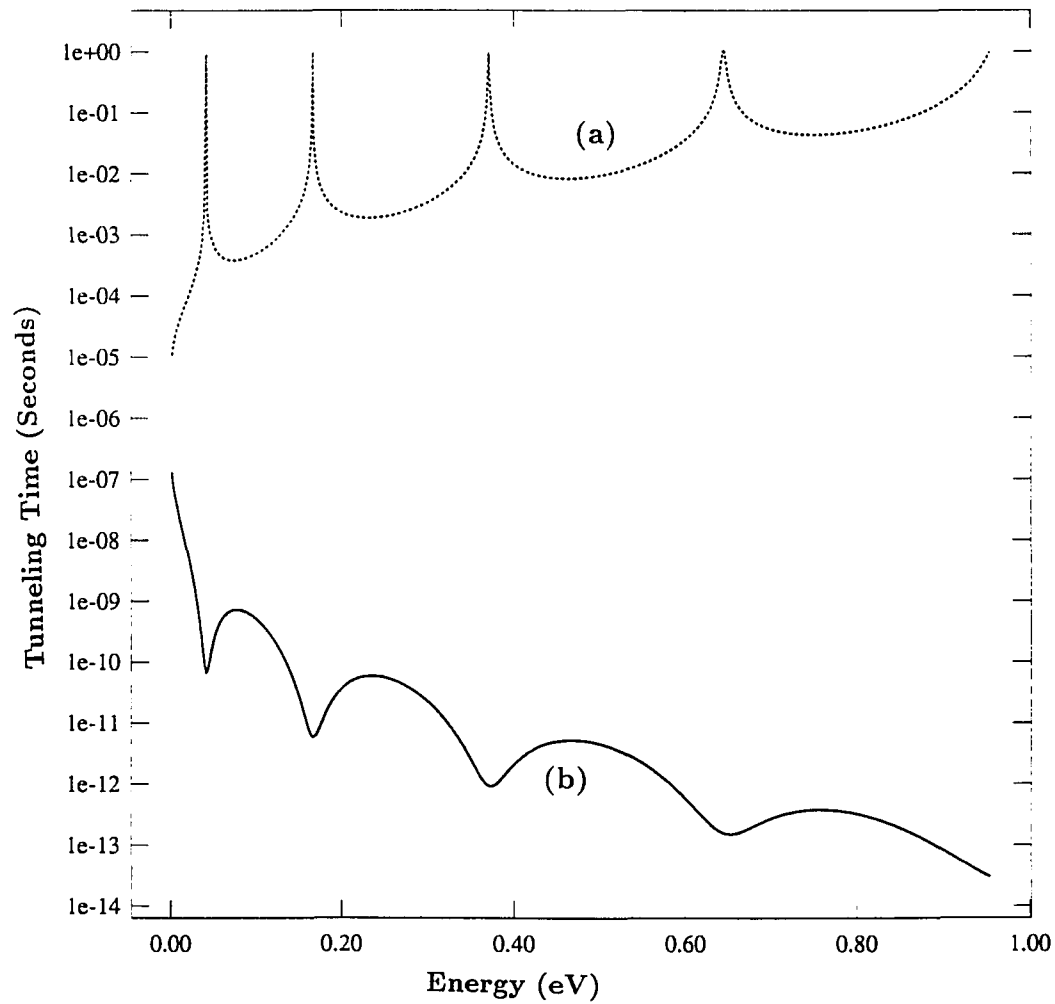


Figure 6.10: Plot of the (a) Transmission Coefficient and the (b) APT time for a symmetrical double rectangular potential barrier structure with a barrier height  $0.956\text{eV}$ , barrier width  $30\text{\AA}$  and a well width  $100\text{\AA}$ , for  $E < V_0$ .

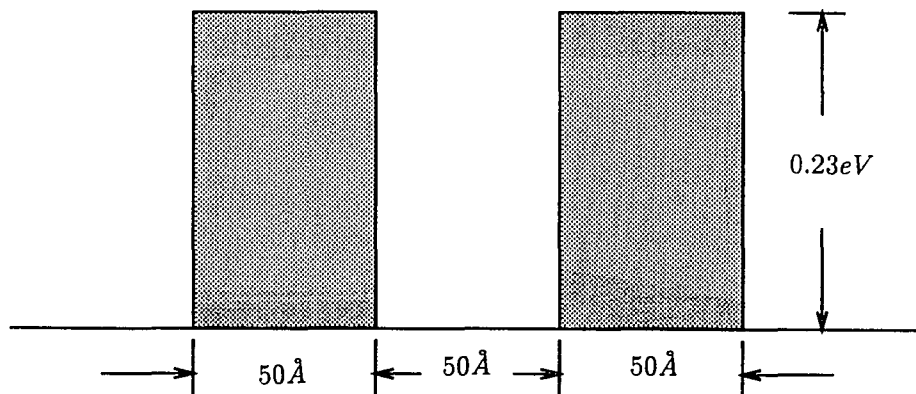


Figure 6.11: The conduction band edge profile of a symmetrical double rectangular potential barrier structure with a barrier height  $0.23\text{eV}$ , barrier width  $50\text{\AA}$  and a well width  $50\text{\AA}$ .

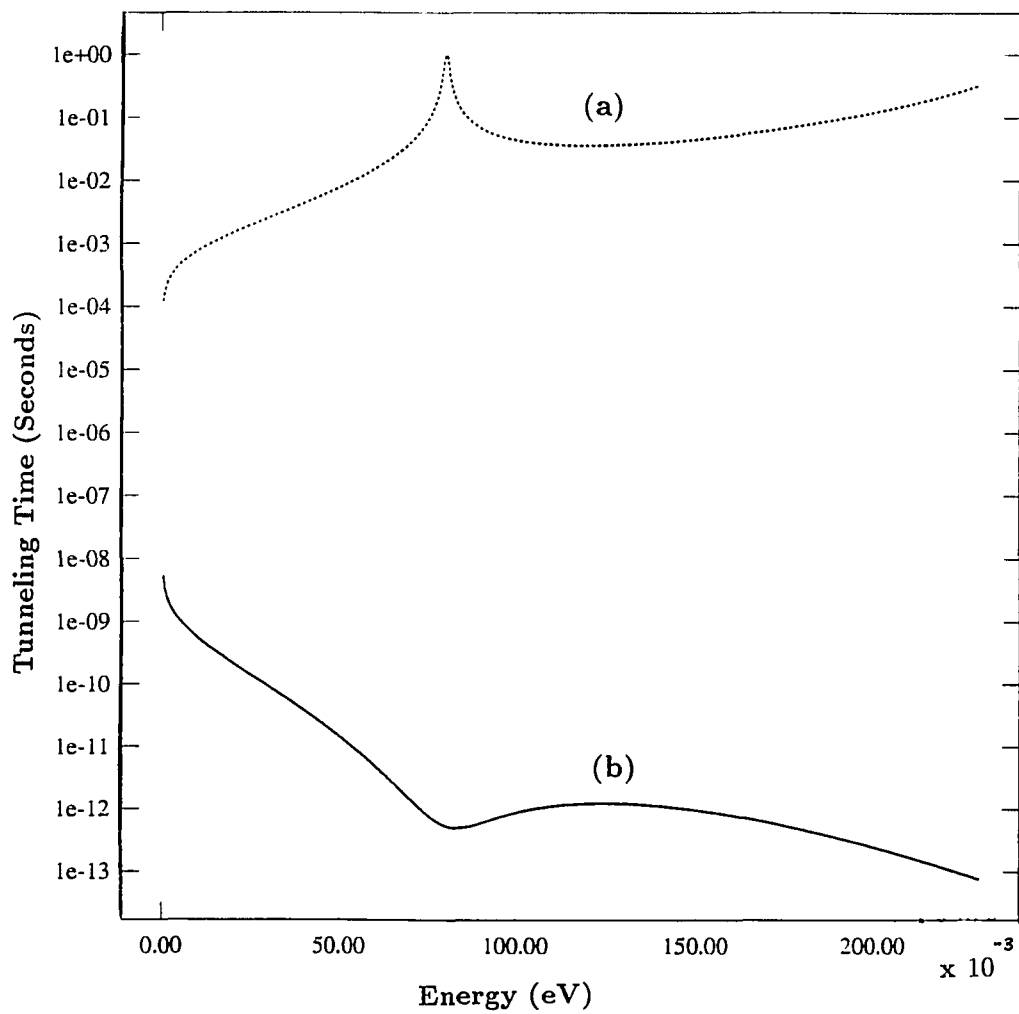


Figure 6.12: Plot of the (a) Transmission Coefficient and the (b) APT time for a symmetrical double rectangular potential barrier structure with a barrier height  $0.23eV$ , barrier width  $50\text{\AA}$  and a well width  $50\text{\AA}$ , for  $E < V_0$ .

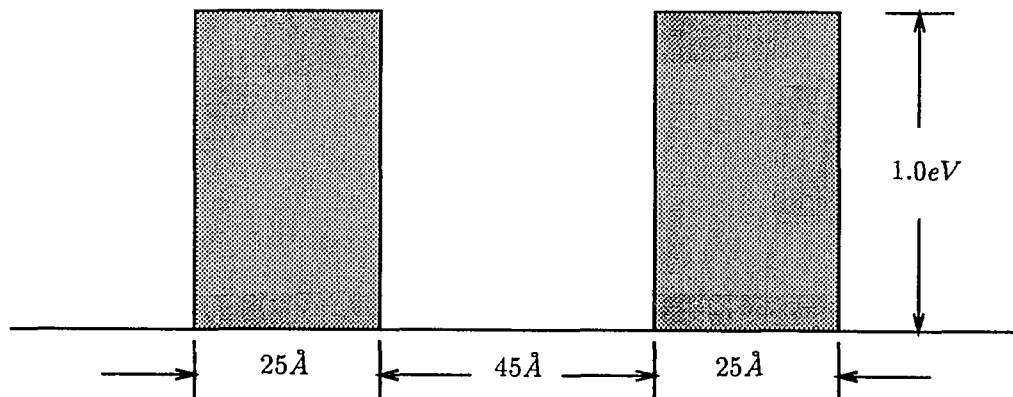


Figure 6.13: The conduction band edge profile of a symmetrical double rectangular potential barrier structure with a barrier height  $1.0eV$ , barrier width  $25\text{\AA}$  and a well width  $45\text{\AA}$ .

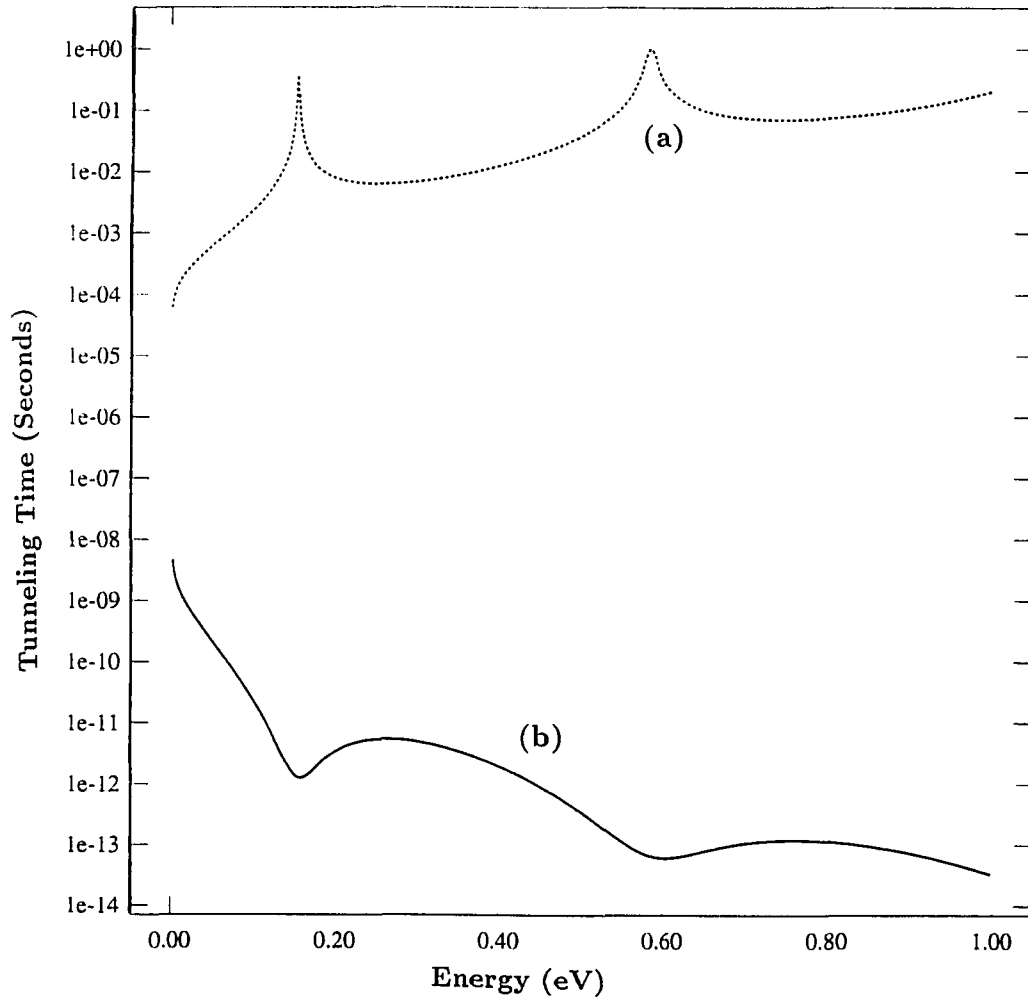


Figure 6.14: Plot of the (a) Transmission Coefficient and the (b) APT time for  $E < V_0$  for a symmetrical double rectangular potential barrier structure with a barrier height  $1.0eV$ , barrier width  $25\text{\AA}$  and a well width  $45\text{\AA}$ .



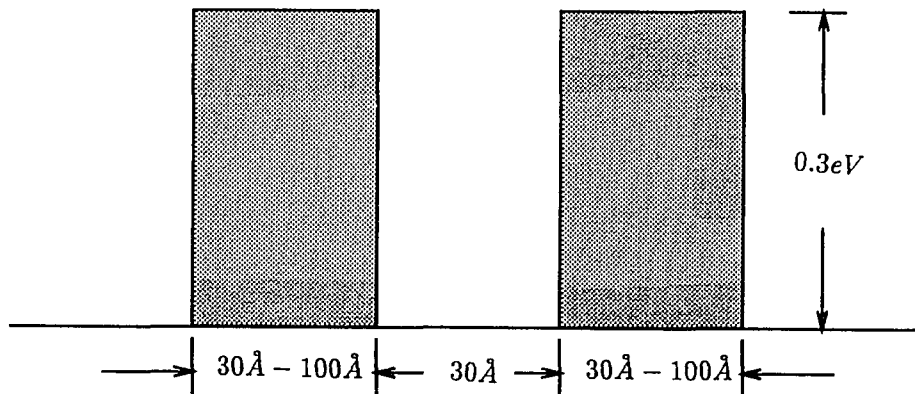


Figure 6.15: The conduction band edge profile of a symmetrical rectangular double potential barrier structure of barrier height  $0.3eV$ , barrier width in the range from  $30\text{\AA}$  to  $100\text{\AA}$  and well width  $30\text{\AA}$ , for  $E < V_o$ .

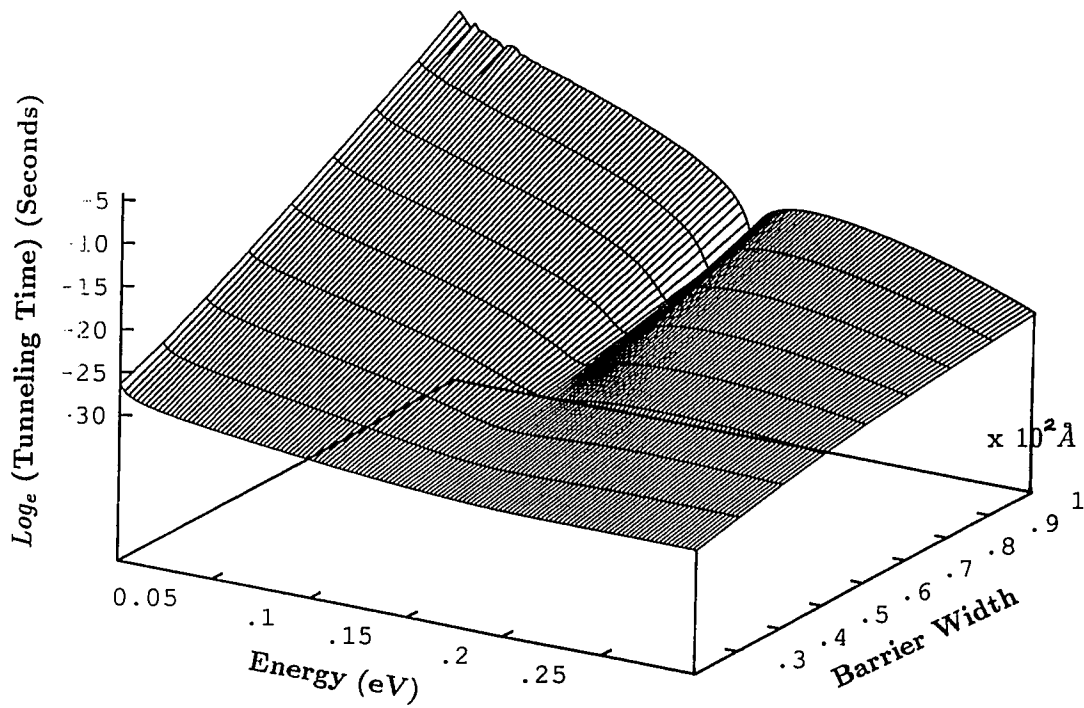


Figure 6.16: 3-Dimensional surface plot of the APT time for  $E < V_0$ . The barrier height is  $0.3\text{eV}$  and the barrier width in the range from  $30\text{\AA}$  to  $100\text{\AA}$  and the well width is  $30\text{\AA}$ .

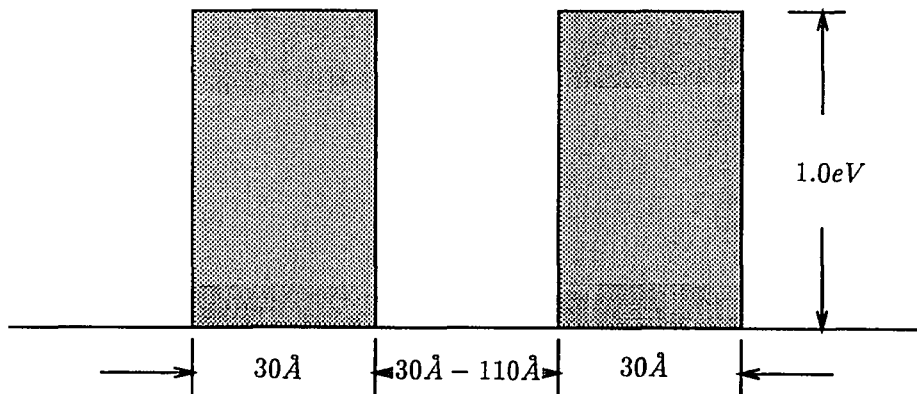


Figure 6.17: The conduction band edge profile of a symmetrical rectangular double potential barrier structure of barrier height  $1.0\text{eV}$ , barrier width  $30\text{\AA}$  and the well width in the range from  $30\text{\AA}$  to  $110\text{\AA}$ .

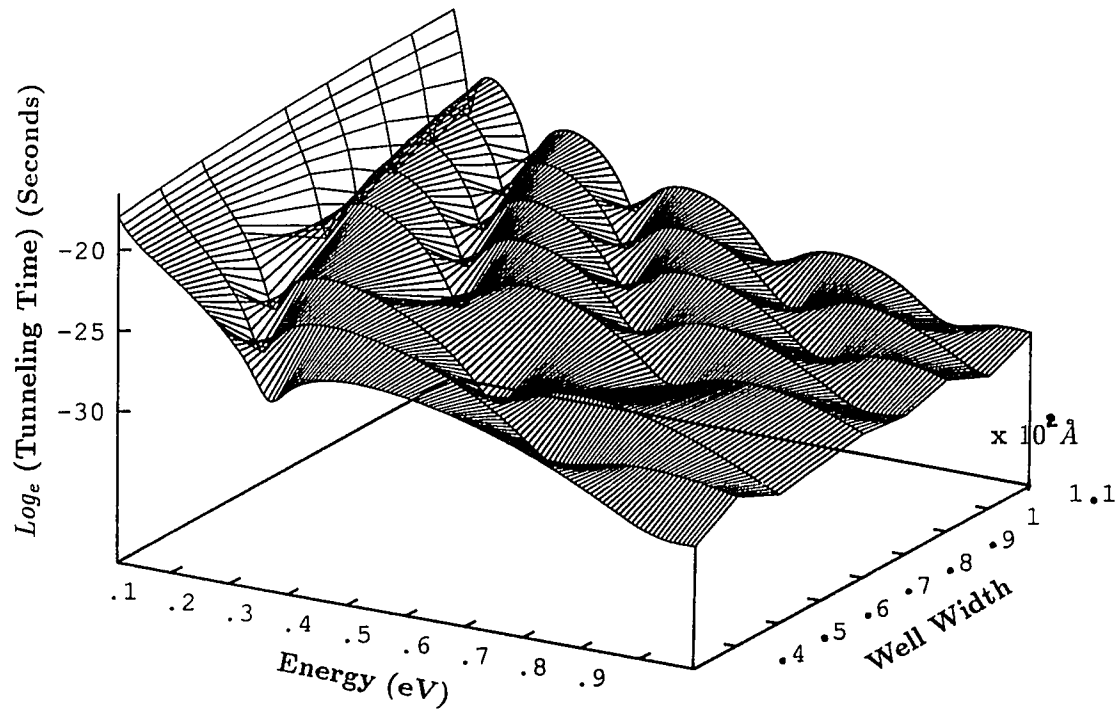


Figure 6.18: 3-Dimensional surface plot of the APT time for  $E < V_0$ . The barrier height is  $1.0\text{eV}$  and barrier width  $30\text{\AA}$  and the well width in the range from  $30\text{\AA}$  to  $110\text{\AA}$ .

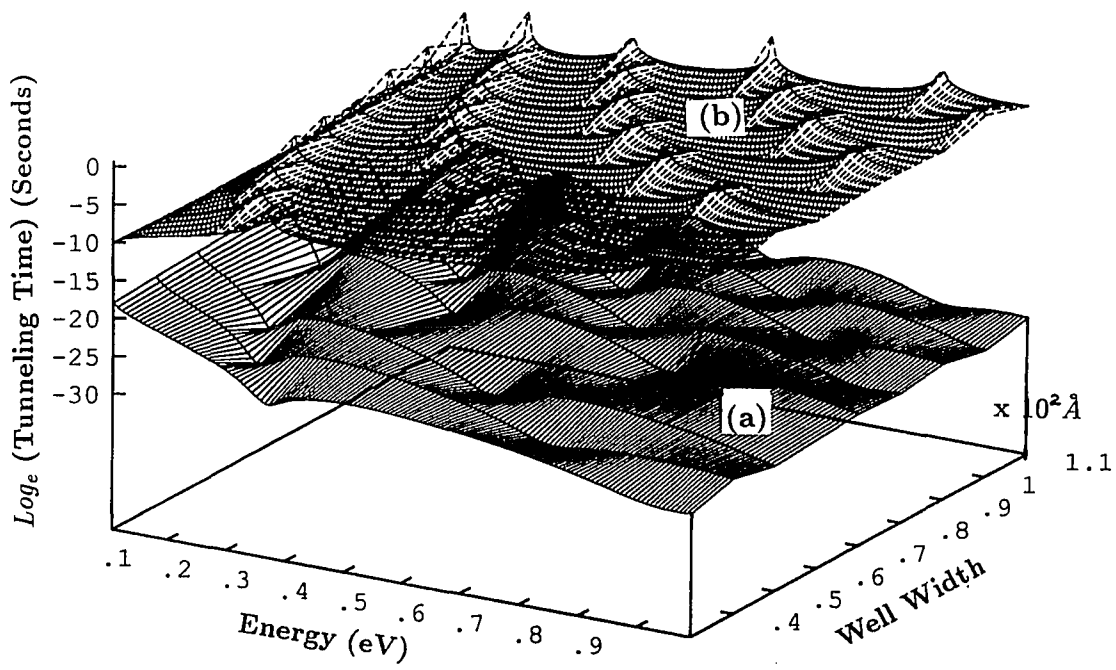


Figure 6.19: 3-Dimensional surface plot of the (a) APT time and the (b) transmission coefficient for  $E < V_0$ . The barrier height is  $1.0\text{eV}$  and barrier width is  $30\text{\AA}$  and well width in the range from  $30\text{\AA}$  to  $110\text{\AA}$ .

## Chapter 7

# CONCLUSION

Starting from the analytical solution to the time-independent Schrödinger equation in one-dimension, and exploiting the analogy between the transmission line equation and the solution to the Schrödinger equation, an analytical expression for the Average Particle Traversal (APT) time,  $\tau_{APT}$ , was derived in terms of the real part of the Quantum Mechanical Wave Impedance (QMWI). This approach was used to derive an analytical expression for the  $\tau_{APT}$  through a single rectangular potential barrier under zero bias, and the results were compared with the dwell time, the phase-delay time, the Buttiker-Landauer time, the Collins-Barker numerical traversal time and the classical traversal time. The APT time is inversely proportional to the transmission coefficient.  $\tau_{APT}$  approaches infinity as the incident energy tends to zero and as the energy goes to infinity,  $\tau_{APT}$  tends to the classical time. The APT time is always more than the classical traversal time. The same approach was extended to obtain an analytical expression for the  $\tau_{APT}$  through a symmetric double rectangular potential barrier structure under zero bias. The APT time is inversely proportional to the transmission coefficient and the  $\tau_{APT}$  attains a minimum at resonant energies when the transmission coefficient is unity. The maximum frequency of oscillation of some of experimentally studied resonant tunneling structures were compared with those obtained using APT time. The agreement is good.

The capacitance charging time at the depletion regions were not taken into consideration. The

effective masses were assumed to be constant throughout the structure. The  $\tau_{APT}$  in the free propagation regions, ahead and beyond the barriers, were not taken into consideration. The effect of the effective mass can be incorporated in this approach and an analytical expression for the  $\tau_{APT}$  for a barrier structure with different outer edges can possibly be derived. An analytical expression can possibly be derived for the  $\tau_{APT}$  through unsymmetrical double potential barriers. Coupled-quantum-wells effect can also be incorporated. As the pre-free-propagating region may play an important role, the traversal time through the pre-free-propagating region also should be considered, especially when comparison with experiments are made.

# Bibliography

- [1] ALAM, M. A., AND KHONDKER, A. An efficient self-consistent model for resonant tunneling structures. *Journal of Applied Physics* 68, 12 (December 1990), 6501–6503.
- [2] ANDO, Y., AND ITOH, T. Calculation of transmission tunneling current across arbitrary potential barriers. *Journal of Applied Physics* 61, 4 (February 1987), 1497–1502.
- [3] ANWAR, A., KHONDKER, A., AND KHAN, M. Calculation of the traversal time in resonant tunneling devices. *Journal of Applied Physics* 65, 7 (April 1989), 2761–2765.
- [4] ANWAR, A., LACOMB, R., , AND CAHAY, M. Influence of impurity scattering on the traversal time and current-voltage characteristics of resonant tunneling structures. *Superlattices and Microstructures* 11, 1 (1992), 131–135.
- [5] BONNEFOI, A., AND CHOW, D. Inverted base-collector tunnel transistor. *Applied Physics Letters* 47, 8 (1985), 888–890.
- [6] BONNEFOI, A., AND MCGILL, T. Resonant tunneling transistors with controllable negative differential resistances. *IEEE Electron Device Letters EDL-6*, 12 (1985), 636–638.
- [7] BUTTIKER, M. Lamor precession and the traversal time for tunneling. *Physical Review B* 27, 10 (May 1983), 6178–6188.
- [8] BUTTIKER, M., AND LANDAUER, R. Traversal time for tunneling. *Physical Review Letters* 49, 23 (December 1982), 1739–1742.



- [9] BUTTIKER, M., AND LANDAUER, R. Traversal time for tunneling. *Physica Scripta* 32 (1985), 429–434.
- [10] BUTTIKER, M., AND LANDAUER, R. Traversal time for tunneling. *IBM Journal of Research and Development* 30, 5 (September 1986), 451–454.
- [11] CAHAY, M., DALTON, K., AND FISHER, G. Tunneling time through resonant tunneling devices and quantum mechanical bistability. *Superlattices and Microstructures* 11, 1 (1992), 113–117.
- [12] CAHAY, M., DICHIARO, T., THANIKASALAM, P., AND VENKATASUBRAMANIAN, R. Quantum mechanical tunneling time and it's relation to Tsu-Esaki formula. *Proceedings of the SPIE Conference, New Jersey* (April 1992).
- [13] CAPASSO, F., AND KIEHL, R. Resonant tunneling transistor with quantum well base and high-energy injection: A new negative differential resistance device. *Journal of Applied Physics* 58, 3 (1985), 1366–1368.
- [14] CAPASSO, F., AND MOHAMMED, K. Quantum photoconductive gain by effective mass filtering and negative conductance in superlattice P-N junctions. *Physica* 134B (1985), 487–493.
- [15] CAPASSO, F., AND MOHAMMED, K. Resonant tunneling through double barriers, perpendicular quantum transport phenomena in superlattices, and their device applications. *IEEE Journal of Quantum Electronics* QE-22, 9 (1986), 1853–1869.
- [16] COLLINS, S., LOWE, D., AND BARKER, J. The quantum mechanical tunneling problem-revisited. *Journal of Physics C: Solid State Physics* 20 (1987), 6213–6232.
- [17] COLLINS, S., LOWE, D., AND BARKER, J. R. A dynamic analysis of resonant tunneling. *Journal of Physics C: Solid State Physics* 20 (1987), 6233–6243.
- [18] COLLINS, S., LOWE, D., AND BARKER, J. R. Resonant tunneling in heterostructures: Numerical simulation and qualitative analysis of the current density. *Journal of Applied Physics* 63, 1 (January 1988), 142–149.

- [19] DE MOURA, M. A., AND DE ALBUQUERQUE, D. F. Remarks on the traversal time in a tunneling process. *Solid State Communications* 74, 5 (1990), 353–354.
- [20] ESAKI, L. Superlattice and negative conductivity in semiconductors. *IBM Research notes RC-2418* (1969).
- [21] ESAKI, L. A bird's eye view on the evolution of semiconductor superlattices and quantum wells. *IEEE Journal of Quantum Electronics QE-22*, 9 (1986), 1611–1624.
- [22] ESAKI, L., HOWARD, L., AND RIDEOUT, V. Transport properties of a GaAs-AlGaAs superlattice. *Proceedings of the 11th International Conference on Physics of Semiconductors, Warsaw, Poland* (1972), 431–436.
- [23] ESAKI, L., AND TSU, R. Superlattice and negative differential conductivity in semiconductors. *IBM Journal of Research and Development* (1970), 61–65.
- [24] GLAZER, Y., AND GITTERMAN, M. Tunneling through highly transparent symmetric double barriers. *Physical Review B* 43, 2 (January 1991), 1855–1858.
- [25] GOODHUE, W., AND SOLLNER, T. Large room-temperature effects from resonant tunneling through AlAs barriers. *Applied Physics Letters* 49, 17 (October 1986), 1086–1088.
- [26] HARTMAN, T. E. Tunneling of a wave packet. *Journal of Applied Physics* 33, 12 (December 1962), 3427–3433.
- [27] HAUGE, E., AND ST, J. Tunneling times: A critical review. *Reviews of Modern Physics* 61, 4 (October 1989), 917–936.
- [28] HUANG, Z., AND CUTLER, P. Model studies of tunneling time. *Journal of Vacuum Science and Technology A* 8, 1 (Jan/Feb 1990), 186–191.
- [29] JAUHO, A. P., AND JONSON, M. Tunneling times in heterostructures. *Superlattices and Microstructures* 6, 3 (1989), 303–307.

- [30] KHONDKER, A. A model for resonant and sequential tunneling in the presence of scattering. *Journal of Applied Physics* 67, 10 (May 1990), 6432–6437.
- [31] KHONDKER, A., KHAN, M., AND ANWAR, A. Transmission line analogy of resonant tunneling phenomena: The generalized impedance concept. *Journal of Applied Physics* 63, 10 (May 1988), 5191–5193.
- [32] LEAVENS, C. Transmission, reflection and dwell times within Bohm's causal interpretation of quantum mechanics. *Solid State Communications* 74 (1990), 923–928.
- [33] LEAVENS, C. Traversal times for rectangular barriers within Bohm's causal interpretation of quantum mechanics. *Solid State Communications* 76, 3 (1990), 253–261.
- [34] LURYI, S., AND CAPASSO, F. Resonant tunneling of two-dimensional electrons through a quantum wire: A negative transconductance device. *Applied Physics Letters* 47, 12 (1985), 1347–1349.
- [35] NAKATA, Y., AND ASADA, M. Analysis of novel resonant electron transfer triode device using metal-insulator superlattice for high speed response. *IEEE Journal of Quantum Electronics* QE-22, 9 (1986), 1880–1886.
- [36] PANDEY, L., AND SAHU, D. Dwell time and average speed in a resonant tunneling structure. *Solid State Communications* 72, 1 (1989), 7–11.
- [37] POLLAK, E. *Journal of Chemical Physics* 83 (1985), 1111.
- [38] POLLAK, E., AND MILLER, W. *Physical Review Letters* 53 (1984), 115.
- [39] RAMAGLIA, V. M., AND TAGLIACCOZZO, A. Magnetic-field-induced resonant tunneling across a thick square barrier. *Physical Review B* 43, 3 (January 1991), 2201–2212.
- [40] RANFAGNI, A., AND MUGNAI, D. Semiclassical tunneling time in presence of dissipation: An optical model. *Physica Scripta* 42 (1990), 508–512.

- [41] RANFAGNI, A., AND MUGNAI, D. Delay-time measurements in narrow wave guides as a test of tunneling. *Applied Physics Letters* 58, 7 (February 1991), 774-776.
- [42] RAY, S., RUDEN, P., AND SOKOLOV, V. Resonant tunneling at 300<sup>0</sup> k in GaAs-AlGaAs quantum wells grown by metalorganic chemical vapor deposition. *Applied Physics Letters* 48, 24 (June 1986), 1666-1668.
- [43] SHEWCHUK, T., CHAPIN, P., AND COLEMAN, P. Resonant tunneling oscillations in GaAs-AlGaAs heterostructure at room temperature. *Applied Physics Letters* 46, 5 (March 1985), 508-510.
- [44] SHEWCHUK, T., CHAPIN, P., AND COLEMAN, P. Stable and unstable current-voltage measurements of a resonant tunneling heterostructure oscillator. *Applied Physics Letters* 47, 9 (November 1985), 986-988.
- [45] SMITH, F. T. Lifetime matrix in collision theory. *Physical Review* 118, 1 (April 1960), 349-356.
- [46] SOKOLOVSKI, D., AND BASKIN, L. *Physical Review A* 36 (1987), 4604.
- [47] SOLLNER, T., BROWN, E., AND GOODHUE, W. Observation of millimeter-wave oscillation from resonant tunneling diodes and some theoretical considerations of ultimate frequency limits. *Applied Physics Letters* 50, 6 (February 1987), 332-334.
- [48] SOLLNER, T., AND GOODHUE, W. Resonant tunneling through quantum wells at frequencies up to 2.5THz. *Applied Physics Letters* 43, 6 (September 1983), 588-590.
- [49] TSUCHIYA, AND MASAHIRO. Room-temperature observation of differential negative resistance in an AlAs/GaAs/AlAs resonant tunneling diode. *Japanese Journal of Applied Physics* 24, 6 (1985), 466-468.
- [50] WIGNER, E. P. Lower limit for the energy derivative of the scattering phase shift. *Physical Review* 98, 1 (April 1955), 145-147.

## Chapter 8

# APPENDIX A

### 8.1 Complex Coefficients of Wave Function Solutions

The complex constants involved in the solutions to the Schrödinger Equation are given in this section.

The suffix 1 and 2 indicate the real and imaginary parts of the constants, respectively.

$$A = \frac{e^{i2kd}}{i2k\alpha e^{\alpha d}} \left( \frac{\alpha + ik}{\alpha - ik} \right) \left[ [(k^2 - \alpha^2) + (\alpha - ik)^2 e^{i2kd_1}] \sinh(\alpha d) + i2k\alpha \cosh(\alpha d) \right] - \left( \frac{\alpha + ik}{\alpha - ik} \right) \quad (8.1)$$

$$B = \frac{H e^{ik2d} (\alpha + ik)}{i4k\alpha^2 e^{\alpha d}} \left[ [(k^2 - \alpha^2) + e^{i2kd_1} (\alpha - ik)^2] \sinh(\alpha d) + i2k\alpha \cosh(\alpha d) \right] \quad (8.2)$$

$$C = \frac{H e^{i2kd} (\alpha - ik)}{i4k\alpha^2 e^{-\alpha d}} \left[ [(k^2 - \alpha^2) + e^{i2kd_1} (\alpha + ik)^2] \sinh(\alpha d) + i2k\alpha \cosh(\alpha d) \right] \quad (8.3)$$

$$D = \frac{H e^{ikd}}{i2k\alpha} [(k^2 - \alpha^2) \sinh(\alpha d) + i2k\alpha \cosh(\alpha d)] \quad (8.4)$$

$$E = \frac{H e^{ik(3d+2d_1)}}{i2k\alpha} (\alpha^2 + k^2) \sinh(\alpha d) \quad (8.5)$$

$$F = \frac{H e^{ik(2d+d_1)}(\alpha + ik)}{2\alpha e^{\alpha(2d+d_1)}} \quad (8.6)$$

$$G = \frac{H e^{ik(2d+d_1)}(\alpha - ik)}{2\alpha e^{-\alpha(2d+d_1)}} \quad (8.7)$$

$$\begin{aligned} B_1 = & \alpha(k^2 - \alpha^2)(1 - e^{-2\alpha d}) \sin^2(kd_1) \\ & + 2\alpha^2 k(1 - e^{-2\alpha d}) \sin(kd_1) \cos(kd_1) \\ & + k(k^2 - \alpha^2)(1 - e^{-2\alpha d}) \sin(kd_1) \cos(kd_1) \\ & + \alpha k^2(1 - e^{-2\alpha d})(1 - 2\sin^2(kd_1)) \\ & - \alpha k^2(1 + e^{-2\alpha d}) \end{aligned} \quad (8.8)$$

$$\begin{aligned} B_2 = & k(k^2 - \alpha^2)(1 - e^{-2\alpha d}) \sin^2(kd_1) \\ & + 2\alpha k^2(1 - e^{-2\alpha d}) \sin(kd_1) \cos(kd_1) \\ & - \alpha(k^2 - \alpha^2)(1 - e^{-2\alpha d}) \sin(kd_1) \cos(kd_1) \\ & - \alpha^2 k(1 - e^{-2\alpha d})(1 - 2\sin^2(kd_1)) \\ & + \alpha^2 k(1 + e^{-2\alpha d}) \end{aligned} \quad (8.9)$$

$$\begin{aligned}
C_1 &= \alpha(k^2 - \alpha^2)(e^{2\alpha d} - 1) \cos^2(kd_1) \\
&\quad - 2\alpha^2 k(e^{2\alpha d} - 1) \sin(kd_1) \cos(kd_1) \\
&\quad + k(k^2 - \alpha^2)(e^{2\alpha d} - 1) \sin(kd_1) \cos(kd_1) \\
&\quad + \alpha k^2(e^{2\alpha d} - 1)(-1 + 2 \cos^2(kd_1)) \\
&\quad + \alpha k^2(e^{2\alpha d} + 1)
\end{aligned} \tag{8.10}$$

$$\begin{aligned}
C_2 &= \alpha(k^2 - \alpha^2)(e^{2\alpha d} - 1) \cos(kd_1) \sin(kd_1) \\
&\quad + 2\alpha k^2(e^{2\alpha d} - 1) \sin(kd_1) \cos(kd_1) \\
&\quad - k(k^2 - \alpha^2)(e^{2\alpha d} - 1) \cos^2(kd_1) \\
&\quad + \alpha^2 k(e^{2\alpha d} - 1)(-1 + 2 \cos^2(kd_1)) \\
&\quad + \alpha^2 k(e^{2\alpha d} + 1)
\end{aligned} \tag{8.11}$$

$$D_1 = \frac{2k\alpha \cos(kd) \cosh(\alpha d) + (k^2 - \alpha^2) \sin(kd) \sinh(\alpha d)}{2k\alpha} \tag{8.12}$$

$$D_2 = \frac{2k\alpha \cosh(\alpha d) \sin(kd) - (k^2 - \alpha^2) \cos(kd) \sinh(\alpha d)}{2k\alpha} \tag{8.13}$$

$$E_1 = \frac{(\alpha^2 + k^2) \sin[k(3d + 2d_1)] \sinh(\alpha d)}{2k\alpha} \tag{8.14}$$

$$E_2 = \frac{-(\alpha^2 + k^2) \cos[k(3d + 2d_1)] \sinh(\alpha d)}{2k\alpha} \quad (8.15)$$

$$F_1 = \frac{\alpha \cos[k(2d + d_1)] - k \sin[k(2d + d_1)]}{2\alpha e^{\alpha(2d+d_1)}} \quad (8.16)$$

$$F_2 = \frac{k \cos[k(2d + d_1)] + \alpha \sin[k(2d + d_1)]}{2\alpha e^{\alpha(2d+d_1)}} \quad (8.17)$$

$$G_1 = \frac{\alpha \cos[k(2d + d_1)] + k \sin[k(2d + d_1)]}{2\alpha e^{-\alpha(2d+d_1)}} \quad (8.18)$$

$$G_2 = \frac{\alpha \sin[k(2d + d_1)] - k \cos[k(2d + d_1)]}{2\alpha e^{-\alpha(2d+d_1)}} \quad (8.19)$$